91602
new 82-10

ontario hydro
research division

COMPLIMENTARY COPY
Please Credit Ontario Hydro Research if
Reproduced in Whole or in Part

TO: Dr. D.P. Dautovich
Program Manager, CFFTP
Design & Development - Gen, Fusion Centre

PHOTOREACTOR DESIGN FOR LASER-BASED TRITIUM SEPARATION

Hugh D. Morrison

A summary of research on photoreactors for tritium separation is presented. The main concern is the development of a photoreactor that utilizes the energy of CO_2 lasers most efficiently to dissociate CF_3T. A figure of merit to assess the efficiency of a photoreactor has been developed specifically for this process. The known characteristics of dissociation of CF_3T and of absorption in CF_3H are reviewed to provide a set of criteria for designing a photoreactor. Three photoreactor designs have been proposed. Two of the designs are suitable for further development. Several spreadsheet programs have been written as tools for designing photoreactors and for estimating the laser power required for a large-scale application. A poster paper of the same title as this report was presented 17 January 1990 at The Institute of Physical and Chemical Research (RIKEN) in Japan. The summary, text and figures of the poster appear in an appendix. Six other appendices provide a detailed technical summary of the spreadsheet programs and of the other mathematical analyses discussed in the report.

1. INTRODUCTION

The research program of laser-based tritium separation at Ontario Hydro Research Division has reached the stage where we must build and test prototype components for the process. One of the crucial components in the process is the photoreactor where the tritium carrying gas, trifluoromethane or CF_3T in CF_3H, interacts with the light from a pulsed CO_2 laser. The interaction results in isotope selective dissociation of the gas. For laser-based tritium separation to compete with other separation technologies the photoreactor must be highly efficient, both in photon utilization and in dissociation efficiency. The problem is not a trivial one given the physical demands that dissociation of CF_3T places on the photoreactor materials and on the lasers. This report reviews the major issues of photoreactor design.

The fundamental issue is the determination of the optimum conditions for selective dissociation of CF_3T. The concentration of the CF_3T is at most a few parts per million. Thus, most of the laser pulse energy is absorbed by the majority species, CF_3H. The energy absorption in CF_3H determines in large part the optimum temperature and pressure. The dissociation and absorption processes also depend non-linearly on the fluence and duration of the laser pulse. Systematic studies of dissociation and absorption under controlled conditions provide the necessary data base to design a photoreactor. Such studies have been performed, some at Ontario Hydro Research Division and many more at other research centres, and the main results are summarized in this report. The development of a prototype photoreactor design will determine the need for more studies.

job	file	date	report no.
16-105	819.312	August 8, 1990	90-121-K

The main design problem of the photoreactor is to implement the dissociation in a continuous process, i.e. combining continuous gas flow with efficient dissociation. Over the course of the research into laser-based tritium separation two design concepts have been examined: an equifluence cell and a cylindrical dielectric waveguide. Recently, a third concept has been suggested, a parallel-plate waveguide. The equifluence cell was originally developed by Vanderleeden for deuterium separation.[1] The initial plans for tritium separation, however, did not require such a large photoreactor. Thus, for small-scale applications the designated photoreactor was a cylindrical dielectric waveguide patented by Dr. J.A. O'Neill.[2] In 1987 the target of the research program shifted to a large-scale application, a plant for tritium production at NET (Next European Torus) to process 500 kg/hr of tritiated light water.[3] As the state of the waveguide concept then was too costly in laser power for this large-scale application, the equifluence cell concept was resurrected. Estimates of the laser power required for the 500 kg/hr plant design have all been based on the equifluence cell. The simple model of this cell employed in the cost analysis considered an ideal case; it neglected the propagation of real laser beams. In January 1990, a poster presentation (see Appendix A) at the Institute for Physical and Chemical Research in Japan introduced a new photoreactor design, a parallel-plate waveguide. This design incorporates the propagation of real beams in a cell designed for large-scale applications.

Construction of a prototype photoreactor requires careful consideration of the materials required, especially for windows and mirrors. This may require a compromise on the optimum dissociation conditions, depending on the properties of the materials available. Another concern for prototype development is matching the specifications of CO_2 lasers to the requirements of the dissociation process. As the technology of CO_2 lasers is well developed, usually the availability of suitable lasers for the process is just assumed. Laser output, however, must match the input requirements of the photoreactor design, so we must also consider the requirements placed on the laser system.

The main aim of this report is to provide a summary of the current state of photoreactor development for laser-based tritium separation. Various tools for analysis, such as beam propagation formulas and spreadsheet programs on computer, are also discussed and included in appendices. Section 2 develops a figure of merit to assess the performance of a photoreactor for tritium production. A second figure of merit obtained directly from the first one applies to tritium removal from a waste stream. To apply the figures of merit we must understand the process of dissociation of CF_3T. Section 3 reviews what is known about CF_3T dissociation from experimental measurements performed at Ontario Hydro Research Division and at other research centres. As CF_3T is usually present in concentrations on the order of 1 ppm, essentially all the energy dissipated in a photoreactor is absorbed by the non-dissociating CF_3H. Section 4 discusses absorption in CF_3H as a function of fluence and of pulse length. Then Section 5 examines various cell designs and reviews their advantages and disadvantages. Two of the cell designs have been incorporated into spreadsheets to analyze the laser power requirements of laser-based tritium separation. These analyses are reviewed in Section 6 and the spreadsheets are described in detail in two appendices. The figures of merit from Section 2 can be calculated from data in these spreadsheets. Section 7 considers the problem of providing lasers to match the requirements of a photoreactor. Finally, Section 8 provides a brief summary with conclusions for future work on photoreactor development.

2. ASSESSING PHOTOREACTOR PERFORMANCE

2.1 Figure of Merit

The problem of photoreactor design is to allow the gas molecules to interact with the pulsed laser beam to achieve a specified level of depletion. To solve this problem we must answer several questions. How does gas flow through the photoreactor (e.g. plug flow or stirred)? What is the average residence time of the gas in the interaction volume of the photoreactor? How much laser energy per pulse and how many pulses are needed to achieve the required level of depletion? What is the distribution of laser energy within the interaction volume of the photoreactor?

To evaluate the answers to these questions we can calculate the efficiency of the photoreactor. A useful figure of merit is the electrical power supplied to the laser to dissociate a given quantity of CF_3T: P_D measured in units of kW/(mol/hr).

$$P_D = 1/(\varepsilon_l\varepsilon_c) \int_V (n_T\sigma_T + n_H\sigma_H)\, \Phi(V)dV\, [t/(fQnV)]\, [N_A/(3.6 \times 10^6)] \quad kW/(mol/hr). \qquad (1)$$

This equation was developed from a similar one given by Marling, Herman and Thomas for deuterium separation.[4] For a laser pulse passing through a given photoreactor, there is a distribution of fluence $\Phi(V)$ that is absorbed according to the concentrations (n_T and n_H) and absorption cross-sections (σ_T and σ_H) of CF_3T and CF_3H. The integral in Eq. 1 yields the energy absorbed per pulse. Dividing the absorbed energy by the cell efficiency, ε_c, provides the total laser energy delivered to the photoreactor. (The cell efficiency consists of two parts: energy absorbed by the photoreactor and energy absorbed by the gas in the photoreactor. If A_c is the absorption factor for the photoreactor and A_g is the absorption factor for the gas, then ε_c is just $A_g(1-A_c)$.) Further division by the wall-plug electrical efficiency of the laser, ε_l, yields the electrical energy supplied to the laser for one pulse. The number of CF_3T molecules dissociated per pulse is given by the product of the feed concentration, f, the level of depletion, Q, the gas density, n, and the interaction volume of the photoreactor, V, all divided by t. The factor t is the average residence time of the molecules in the photoreactor, measured in number of pulses, to achieve the level of depletion. The final factors, $N_A/(3.6 \times 10^6)$, convert P_D from J/molecule to kw/(mol/hr).

Equation 1 can be simplified by dividing n_T and n_H through by n to yield f and 1–f, respectively. Furthermore, extracting the factor of σ_H within the absorption integral leaves the absorption cross-section of CF_3T expressed by its absorption selectivity over CF_3H,

$$S = S(p,T,\Phi) = \sigma_T(p,T,\Phi) / \sigma_H(p,T,\Phi)\,. \qquad (2)$$

Thus, we now have

$$P_D = 1/(\varepsilon_l\varepsilon_c)\, (1/V) \int_V (fS + 1-f)\, \sigma_H\Phi(V)dV\, [t/(fQ)]\, [N_A/(3.6 \times 10^6)] \quad kW/(mol/hr). \qquad (3)$$

For f on the order of 10^{-6} and S on the order of 10^4 we can neglect fS and f with respect to 1 and write

$$P_D \approx 1/(\varepsilon_l\varepsilon_c)\, (1/V) \int_V \sigma_H\Phi(V)dV\, [t/(fQ)]\, [N_A/(3.6 \times 10^6)] \quad kW/(mol/hr)\,. \qquad (4)$$

Another figure of merit derived from Eq. 1 is more appropriate to the problem of tritium removal rather than tritium production, i.e. the electrical power required to process a given quantity of feed material,

$$P_F = P_D\, f\, Q \quad kW/(mol/hr), \text{ or} \qquad (5)$$

$$P_F \approx 1/(\varepsilon_l\varepsilon_c)\, (1/V) \int_V \sigma_H\Phi(V)dV\, [tN_A/(3.6 \times 10^6)] \quad kW/(mol/hr).$$

If F is the total feed rate to the process, then $\varepsilon_l F P_F$ is the total laser power required by the process. Note that P_F remains dependent on the depletion Q implicitly through the factor t, but is independent of the feed concentration. To see this more clearly let us examine t in more detail.

2.2 Residence Time of Gas in a Photoreactor

The number of pulses t required to achieve a given depletion Q depends on the probability of dissociation per pulse, q, and on the conditions of gas flow through the photoreactor. Fundamental research provides the probability of dissociation as a function of laser fluence, $q(\Phi)$, and on the temperature and pressure of the gas. The flow of gas through the photoreactor determines how dissociation accumulates over several pulses to produce a given depletion. Gas continuously enters and leaves the photoreactor, but on the time-scale of a laser pulse the gas flow is effectively fixed in space. Thus, the gas appears to move only between pulses. The two limiting cases of gas movement are plug flow, in which there is no mixing of the gas from entrance to exit of the photoreactor, and stirred flow, in which the gas is completely mixed between pulses. Plug flow establishes a gradient of depleted gas in the flow stream through the photoreactor, while stirred flow maintains a constant level of depletion throughout the photoreactor. The formulas are developed in Appendix B and listed here:

$$t = \ln(1-Q) / \ln(1-\varepsilon_v) \quad \text{for plug flow,} \tag{6a}$$

$$t = Q(1-\varepsilon_v) / [(1-Q)\varepsilon_v] \quad \text{for stirred flow,} \tag{6b}$$

where ε_v is the effective probability of dissociation per pulse. Figure 1 shows a sample calculation of t as a function of ε_v for three values of Q in the two cases. Obviously, fewer pulses are required to achieve a given depletion with plug flow than with stirred flow. Therefore, a good design for a photoreactor should incorporate plug flow as much as possible.

2.3 Other Factors in Figure of Merit

What other factors in Eq. 1 are affected by the design of the photoreactor? The gas density is determined by the temperature and pressure in the photoreactor. The quantity of energy absorbed depends on the gas density through the pressure and temperature dependence of the absorption cross-section of CF_3H mostly. The cell efficiency ε_c is the ratio of the laser energy absorbed in the gas to the total laser energy delivered to the photoreactor. Thus, for a fixed path length ε_c also depends on gas density through the absorption length coefficient, which is the product of gas density and absorption cross-section. For a higher gas density the energy absorbed can be kept constant by reducing the path length of the laser beam in the photoreactor. Thus, the design of the photoreactor depends greatly on the choice of gas conditions. A range of near optimal conditions should be determined from fundamental experiments in advance of photoreactor design. Prototype development, however, will be a better testing ground.

3. DISSOCIATION OF CF_3T

3.1 Summary of Experimental Results

Now that we have a figure of merit for assessing the performance of photoreactors let us review some of the results of dissociation of CF_3T. The most intensive research on dissociation of CF_3T has been performed by two groups: one with Dr. Kazuo Takeuchi at the Institute for Physical and Chemical Research (RIKEN) in Japan, and another with Dr. Irving Herman at Lawrence Livermore National Laboratories in the United States. A recent publication by Herman, Takeuchi and Makide reviews the topic of tritium separation by laser, covering most of the activities in this field, and provides an extensive list of references to work on CF_3T and many other molecules.[5] The main results for CF_3T are listed here.

- The dissociation rate of CF_3T and of CF_3H is independent of the concentration of CF_3T from 0.01 ppm to 10 ppm.[6]
- Cooling the gas mixture to -78°C from 25°C greatly enhances the selectivity for dissociation of CF_3T over CF_3H.[7] Selectivities greater than 10 000 were observed for pressures from 85 to 205 torr.
- Highest selectivity is obtained at the 9P(8) line (1057 cm^{-1}) of the CO_2 laser.[7,8]
- The 9R(14) CO_2 line at 1075 cm^{-1} provides a lower selectivity but a higher dissociation rate for CF_3T.[8]
- The critical fluence for dissociation is about 60 J/cm^2 for a long laser pulse, and 12 J/cm^2 for a 2-ns laser pulse.[9,10]
- The optimum pressure for minimizing the critical fluence is in the range of 50 to 100 torr and depends on the temperature and the laser pulse duration.[9,10]

This list of experimental results is not meant to be exhaustive, however it does indicate most of the conditions essential for efficient dissociation.

The report of fluence dependence on pulse length in Ref. 9 has been extended by our measurements at Research Division.[11] Figure 1 shows the measured specific dissociation rates plotted as a function of the pulse energy. The variation in pulse length was achieved by three methods. The long pulse is the natural output of the TEA CO_2 laser: a gain-switched spike about 80 ns long followed by a lower intensity tail of about 1 μs duration. The 75-ns long pulse is obtained by minimizing the nitrogen gas content of the laser gas mixture, essentially removing the tail of the long pulse. The shorter pulses were all obtained by electro-optically switching out a portion of the gain-switched spike, and then amplifying that portion if necessary. The 2-ns and 10-ns pulses were roughly rectangular in shape, but the 50-ns pulse had a triangular shape, a steep rise followed by a slow fall down the back side of the gain-switched spike and a sharp cutoff.

Note that as the pulse length decreases the rate of dissociation increases for the same pulse energy. From the raw data in Figure 1 and a suitable theoretical model, the fluence required for dissociation can be determined. Two models are described in detail in Appendix C: the simple dissociation threshold (SDT) model, and the cumulative log normal distribution (CLND) model.[12] The application of the SDT model to the data in Fig. 1 provides the critical fluences for dissociation listed in Table I.

Table I. Critical fluence for dissociation of CF_3T as a function of pulse length.

Pulse Length (ns)	Critical Fluence (J/cm^2)
2 and 10	15 ± 1.1
50	20
75	31 ± 1.6
1000	38 ± 3.0

3.2 Implications for Photoreactor Design

The most important result from the viewpoint of photoreactor design is the fluence required for dissociation. All the critical fluences listed in Table I are higher than for most other molecules, and so the dissociation of CF_3T requires more careful manipulation of the laser beam. For example, 12 J/cm^2 in a 2-ns pulse exceeds the damage threshold of window and mirror materials. The damage threshold for mirrors, however, increases at a rate proportional to the square root of the pulse duration. This rate is faster than the rate of increase in critical fluence shown in Table I. Thus, pulses longer than 2 ns will allow more compact photoreactor designs simply because the windows and mirrors can be closer to the region of dissociation where the laser fluence is high.

The selection of the optimum pulse length for practical LIS will depend not only on the properties of CF_3T and mirror materials but also on the pulse production method. This topic is discussed in more detail in Section 7 where CO_2 laser designs are examined.

It is encouraging that the dissociation of CF_3T is independent of its concentration. This means that we do not have to worry about concentration gradients in the design of the photoreactor. Furthermore, one design will handle a wide range of input concentrations.

Cooling the gas is essential for high selectivity. The only significant source of heat is the laser beam absorption in the CF_3H, discussed in more detail in Section 4. The minimum cooling power required is the amount of laser power consumed by the photoreactor; from Section 2.1 that is $(\varepsilon_c+A_c)\varepsilon_1 FP_F$.

There is an apparent paradox here stemming from the very low concentration of CF_3T. High efficiency demands the consumption of most of the laser power by the gas within the photoreactor. The main sink of the laser power, however, is in the majority species CF_3H. To achieve high selectivity in dissociation the absorption by CF_3H must be minimized. The resolution of the paradox lies in maximizing the volume of the photoreactor where there is efficient dissociation of CF_3T and minimizing the volume where the only interaction is absorption by CF_3H. Therein lies the problem of photoreactor design for dissociation of CF_3T. Now let us examine the absorption properties of CF_3H.

4. ABSORPTION IN CF_3H

Some measurements by Takeuchi and his group suggested that the absorption of CO_2 laser energy by CF_3H was independent of fluence.[13] Measurements made here at Research Division in April 1989 tell a different story. Figure 2 shows the absorption coefficient of the 9R(14) CO_2 laser line in CF_3H at 197 K, as a function of pressure from 0 to 800 torr. Up to 20 J/cm^2 the absorption coefficient is identical with the small-signal absorption obtained at low fluence. The small-signal absorption, indicated by the solid curve, was later confirmed with a low power cw CO_2 laser.[14] The solid curve is a least squares quadratic fit through the origin; the expression is given in Eq. F.3 of Appendix F. Higher fluences with the pulsed laser show significantly higher absorption beginning at about 20 torr. The pulse shape for all the data points above the solid line was a single longitudinal mode, single transverse mode, 1-μs long pulse. Most of the increase in absorption probably occurs in the tail of the pulse, based on observations in December 1989 by L. Pateopol and B. Pogue (graduate students of Dr. O'Neill).

A related comment on the absorption at high pressure is found in Ref. 7. Takeuchi suggests that selective dissociation deteriorates at high pressure because of absorption by CF_3H molecules in hot bands excited during the duration of the 1-μs long laser pulse. That is, during the laser pulse many CF_3H molecules are excited to higher levels, the hot bands, and the population in the hot bands has a greater absorption than the ground state molecules. Therefore, continued excitation of the CF_3H in the hot bands leads to dissociation of CF_3H and that reduces the selectivity for dissociation of CF_3T.

Some pulses of 2 ns duration, but fluences less than 20 J/cm^2, were also used in the absorption measurements shown in Figure 2. These data are consistent with the small-signal absorption. Certainly more measurements of absorption in CF_3H as a function of pulse length and fluence are necessary before we can proceed much further with photoreactor design.

Two other observations of the laser beam absorption in CF_3H with long pulses are important. Measurements of the absorption by a multi-mode beam (many longitudinal modes, single transverse mode) demonstrate 20% less absorption than the single mode beam. This is a surprising result because the greater frequency bandwidth of the multi-mode beam should see less saturation than the single mode beam. If multi-mode beams are just as useful for dissociation as single mode beams then we should be using multi-mode beams. The second observation was that the fluence does not affect the beam shape over the length of the cell (56 cm), i.e. there is no strong evidence of self-focusing or self-defocusing in CF_3H. This agrees with comments made by Dr. S.L. Chin of Laval University on one of his visits to Research Division. On the other hand, he has reported strong self-focusing and self-defocusing found in pure CF_3D. Therefore, we may expect to use long path lengths in a photoreactor filled with CF_3H without distorting the beam. Of course this must be tested.

From the low-signal absorption in Fig. 2, the absorption path length (1/e reduction in intensity) is in the range of 50 to 20 m for pressures between 40 and 100 torr. Such long paths require refocusing or beam confinement (waveguiding) in the photoreactor. Both options will be discussed in Section 5. In both cases a gaussian beam (TEM_{00}) is the preferred shape for the beam cross-section. One problem that may defeat the use of long path lengths in a multipass geometry is the shock wave produced by the absorption in the gas.

5. PHOTOREACTOR DESIGNS

5.1 Entrance Windows for Photoreactors

How does the laser beam enter the photoreactor and what is the window material? The answers to these questions are common to the design of all photoreactors. The primary reason for this is that the fluence required for dissociation greatly exceeds the damage threshold of window materials, typically less than 10 J/cm^2. It is not apparent from the literature if window materials, e.g. crystals of sodium chloride, have damage thresholds that scale as the square root of the pulse duration like metal mirrors do. Every photoreactor must admit a low fluence beam through a window and then condense the beam to provide the much greater fluence required in the interaction

volume. Thus, the design of the entrance section of the photoreactor can be considered separately from the problem of how to design the interaction volume for dissociation.

One idea to circumvent the damage problems of crystalline materials is to employ a gas window, a curtain of fast-flowing gas. Besides the added complexity of this concept, there are two main objections to the gas window: the gas from the window will contaminate the gas in the photoreactor, and containment of tritium bearing molecules is much more difficult than with a solid window. As there has been no concerted effort to develop gas windows for other applications, adding this problem on to the already difficult problem of photoreactor design is an unwarranted complication.

The best window materials are crystals of sodium chloride or potassium chloride. Other materials such as zinc selenide are also possible, but they are much more expensive than the salt windows and suffer from a higher refractive index: an anti-reflection coating is required to reduce Fresnel reflection losses.

The problem of condensing the beam after passing through the window is essentially the problem of mode-matching the laser beam from outside the photoreactor into the interaction volume. As this path passes through CF_3H we would like the path length to be as short as possible to minimize the absorption. No significant dissociation will take place along this path length, so any laser energy absorbed here is just wasted. The shortest path requires a minimum of two focusing elements, probably metal mirrors, to act as a telescope for the beam from the laser into the photoreactor. The first mirror focuses the beam through the window, and the second mirror directs the beam into the interaction volume. Research Report E87-23-K provides a framework for solving this mode-matching problem.[15] It requires a knowledge of the parameters of the laser beam just before the photoreactor and at the entrance to the interaction volume within the photoreactor.

5.2 History of Photoreactor Designs

Fundamental research of multiphoton dissociation at high fluences has been carried out with three types of photoreactor designs. The simplest is the batch cell in a focused geometry, used for almost all dissociation experiments at some time. In a batch cell the focal volume where the fluence is sufficiently high for dissociation is a small fraction ($\sim 10^{-4}$) of the total cell volume. An effort to increase the available focal volume prompted the development of the cylindrical waveguide cell by O'Neill.[2] Another approach by Lupo and Quack employed a mirror inside a cell to collimate a laser beam at high fluence in a double pass.[16] This is essentially the concept of the entrance telescope discussed in Section 5.1 above.

The recent review of tritium separation refers to only two developments in photoreactor design.[5] The first is the continuously stirred reactor developed by Takeuchi and his group.[17] The second is the cylindrical waveguide of O'Neill, which is described further in Section 5.4 below. The photoreactor developed by Takeuchi employed a simple arrangement of one lens to focus a laser beam into the middle of a long cell, followed by two similar cells. The lenses served a second purpose as the windows of the cells. This type of arrangement is very lossy because the fluence is too low for dissociation along most of the path length. To minimize the absorption losses, the number of window sections should be kept to a minimum. This applies to any photoreactor design.

The only photoreactor concept to date that was specifically designed for large-scale development of LIS was the equifluence cell design of Vanderleeden.[1] This design is described in the next section.

5.3 Equifluence Cell

The equifluence cell design for an LIS photoreactor treats the case of many laser beams entering one cell. The combined laser beams form an annulus that sweeps out the entire volume of the cell in a sequence of reflections from internal annular mirrors. The mirrors refocus the beam to compensate for the absorption losses and so maintain the fluence of the beam. Thus, the fluence is equal everywhere in the cell: an equifluence distribution. In theory, almost the entire energy of the laser beams can be consumed in the cell simply by having enough mirrors and passes through the cell. Unfortunately, the equifluence cell design neglects the diffraction effects of real beams. The hard

edges of the mirrors result in significant diffraction losses of the beams, and distort the equifluence distribution. The concept of the equifluence cell, however, is very useful for estimating the theoretical minimum laser power required for an LIS process. Simply keep in mind that an equifluence cell performs better than any real cell.

5.4 Cylindrical Waveguide

As mentioned in Section 5.2, the cylindrical waveguide cell was developed to increase the volume of high fluence available for dissociation. The basic concept is to focus a low-fluence beam through a window and couple the beam into a low loss mode of the waveguide. Appendix D reviews the theory of coupling a gaussian laser beam into a cylindrical waveguide. The material for the waveguide is important; dielectrics, e.g. glass, provide much lower propagation losses than metals. The lowest loss modes in a dielectric cylinder are linearly polarized with a field profile given by Bessel functions of order zero. A gaussian beam couples very efficiently into these modes. One important feature of these modes is that the beam intensity is zero at the wall of the waveguide. Thus, the damage threshold of the waveguide material is not a problem. The only limit on the fluence at the entrance to the cylinder is the breakdown threshold for ionization of the gas itself.

Experimental work with cylindrical waveguides did demonstrate a significant enhancement in the effective volume of dissociation.[2] Alignment of the laser beam, however, to provide optimum coupling into the waveguide was both critical and difficult. Furthermore, there was evidence of coupling into more than one mode that resulted in mode beating and a non-uniform spatial distribution of fluence along the waveguide. Some theoretical work on the cylindrical waveguide has indicated that the presence of the higher order modes can not be neglected (see Appendix D).

The original cylindrical waveguide design only admits gas flow along the length of the cell. This is not a problem for short cells, or low gas flow rates. For high gas flow rates, however, there is a possibility of a significant pressure drop between the entrance and exit of the waveguide. Quantitative analysis of the size of pressure drop for a given gas flow is discussed in Appendix G. A change in the pressure of the gas in a cylindrical waveguide would change the absorption and dissociation characteristics of the gas along the waveguide. This mean that the optimum conditions for dissociation in the cylindrical waveguide would be a function of the gas flow rate, adding an extra degree of complexity to the design.

The maximum useful length of a cylindrical waveguide is at the point where the peak fluence is too low for dissociation. In terms of the SDT model, this occurs when the peak fluence is equal to the critical fluence for dissociation. There is no comparable sharp cut-off in the CLND model, but a similar criterion could be defined, e.g. at half of the saturation fluence. At this point in the cylindrical waveguide, there may still be too much energy in the beam to just throw away. To employ more of this energy for dissociation the beam may be refocused into a smaller waveguide. Another potential solution is to taper the waveguide, but this also constricts the gas flow and increases the pressure drop.

5.5 Parallel-Plate Waveguide in a Multipass Cell

The parallel-plate waveguide is a new design, and no working model has been constructed yet. It was conceived as a method of combining beam confinement and high gas flow rates. A poster paper describing the design appears in Appendix A. The geometry of the design is essentially two rectangular metal plates spaced a distance "2a" apart. In terms of three orthogonal axes, x, y and z, the plates form two y-z planes at x=-a and x=a. The plates act as a waveguide in the x-dimension for a laser beam propagating approximately parallel to the z axis. In the y-direction the beam propagates as if in free space. Mirrors between the plates at both ends direct the beam in multiple passes. The mirrors must have cylindrical surfaces to refocus the beam in the y-direction. Gas flow is transverse to the direction of beam propagation, i.e. along the y-direction. This will allow gas flow at high velocities with negligible pressure drop across the photoreactor.

As in the cylindrical waveguide, there are low loss modes of propagation for linearly polarized beams in the parallel-plate waveguide. Appendix D describes the conditions necessary for coupling a gaussian beam into the lowest order

modes of the parallel-plate waveguide. The lowest loss requires plates made of metal rather than glass as in the cylindrical waveguide. Metal also provides greater thermal conductivity than glass, an important factor for extracting the heat dumped into the gas by the laser beam.

The design of the parallel-plate waveguide is similar to the equifluence cell concept embodied in the spreadsheet EQCELL.WR1 described in Appendix F. Both employ transverse gas flow and multiple passes of a laser beam reflecting from internal mirrors. A spreadsheet to design the mirrors and analyze the beam parameters for the parallel-plate waveguide is described in Appendix E.

5.6 Comparison of Waveguide Designs

The two waveguides described above both provide nearly ideal gas flow, i.e. plug flow. This will be the case in any photoreactor design where the laser beam is physically confined, because then the gas flow is confined too. The two waveguides differ, however, in the direction of gas flow with respect to the direction of beam propagation: one is parallel and the other is transverse. Transverse flow offers a larger cross-sectional area and a shorter path length for the gas through the photoreactor, hence a much greater gas flow rate for the same pressure difference between inlet and outlet. A higher rate of gas flow also implies that fewer photoreactor modules will be required with this design than with the cylindrical waveguide, offering a potential savings in capital and operating costs.

The calculations for the poster summarized in Appendix A employed the CLND model to determine the average probability of dissociation for the fluence distributions in three photoreactor designs: a cylindrical waveguide, a parallel-plate waveguide, and an open cell. The open cell is essentially a cylinder with a diameter much greater than the input beam, to minimize diffraction and to avoid waveguiding (see also Appendix E). The results appear in the graph in Slide 7 of Appendix A. The calculations assumed a fixed cell length (much shorter than the 1/e absorption length) in a single pass, and the same peak fluence at each cell entrance from the same input energy in a gaussian beam. Slide 7 shows a plot of the total dissociation probability for each photoreactor as a function of the ratio of the peak fluence on input to the saturation fluence parameter in the CLND model. Clearly the cylindrical waveguide is superior in this comparison. If the gas flow could be improved then the cylindrical waveguide could be the best choice for the photoreactor design. To compare the performance of these three designs to the ideal equifluence cell note that for a fluence ratio of unity the probability of dissociation is 0.5 (see Appendix C).

A more detailed look at the calculations for Slide 7 reveals that the differences between the three designs here is solely due to the differences in wasted volume, i.e. the volume where no dissociation occurs. A calculation according to Eq. B.1 reveals that the three cells have practically identical volumes of dissociation. Thus Slide 7 clearly demonstrates the effect on efficiency of utilizing as much of the photoreactor volume for dissociation as possible.

This comparison of a single pass over a short length, however, does not fully assess the potential of multiple passes in either the open cell or the parallel-plate waveguide. Only a small fraction of the input beam energy was consumed. A proper comparison of the three designs should examine the case where the input laser beam energy is nearly exhausted. This would include the possibility of overlapping some portion of successive passes of the beam in the multipass geometries.

6. ANALYSES OF LASER POWER REQUIREMENTS

6.1 A Large Scale Application for Tritium Separation

Since 1987 the aim of the research program has been to design a tritium separation plant that could be used for tritium production at NET, a fusion reactor test facility that is still in the design stage. The design parameters for tritium separation are to process 500 kg/hr of light water from 10 Ci/kg down to 1 Ci/kg. A conceptual design of a laser-based tritium separation plant for this application was presented at an international conference on fusion in 1988.[3] The front end of the plant is a chemical exchange process to transfer tritium from the feed water to the

working molecule, CF_3H. From an analysis of the exchange process, we calculate that a flow rate of about 38400 mol/hr of CF_3H is required. If the operating conditions of the photoreactor are a temperature of 198 K and a pressure of 60 torr, then the volumetric flow rate is about 2200 L/s. Probably one photoreactor cannot handle this gas flow, so a modular design of several identical photoreactors operating in parallel is necessary. The assumption of modular units for the photoreactor is an essential element of the laser power analyses described in Appendices F and G and reviewed in the next two sections.

6.2 Equifluence Cell

As mentioned above, the equifluence cell is an ideal geometry for consuming laser energy in the dissociation of CF_3T. Thus, an estimate of the laser power required for the 500 kg/hr plant based on using the equifluence cell represents a theoretical minimum laser power. Real photoreactors will require more laser power to accomplish the same task. The spreadsheet EQCELL.WR1 provides the framework for calculating the laser power used by an equifluence cell. See Appendix F for a detailed description of this spreadsheet.

Table II lists the optical laser power and the figure of merit from Eq. 1 as a function of ε_V, the effective probability of dissociation per pulse. The principal conditions selected for this example are a gas pressure of 200 torr, temperature of 198 K, and Φ_C of 31 J/cm^2 obtained from Table I. The other conditions are as listed in the example found in Appendix F. The laser power in Table II is the optical power entering the interaction volume of the photoreactor, neglecting any losses in the window section. The figure of merit in Table II is calculated assuming an electrical efficiency of 0.02, corresponding to a 75-ns pulse (low nitrogen in the laser gas mixture) at the 9R(14) CO_2 line (see Section 7).

Table II. Laser power required for 500 kg/hr plant using the equifluence cell design as a function of effective probability of dissociation. See text for operating conditions.

ε_V	Optical Power (kW)	P_F (kW/mol/hr)
0.1	813	1.059
0.2	384	0.500
0.5	124	0.161
0.9	37	0.048

Using ε_V as an input variable corresponds to fixing Φ_C as the laser fluence and varying the saturation fluence parameter in the CLND model. In this way the SDT model incorporated in the spreadsheet can effectively operate as the more realistic CLND model (see Appendix C). Strict interpretation of the SDT model would require $\varepsilon_V = 1$.

The minimum required laser power from this example is 37 kW. This is the average optical power from pulsed CO_2 lasers to process the trifluoromethane at the given feed rate of 38,375 mol/hr. As the equifluence cell design represents the theoretical optimum design, the actual laser requirements will be higher. How much higher is a question to be answered by building and testing a prototype photoreactor.

The number of photoreactors selected for the sample solution shown in Appendix F is totally arbitrary. It can be varied to match the requirement for laser power with the size of commercially available lasers. The assumption here is that each photoreactor module will require one laser. Of course, schemes for multiplexing the output of several lasers as input for one photoreactor are also possible.

6.3 Cylindrical Waveguide

The forerunner to EQCELL.WR1 was SEPCOST.WR1 (see Appendix G), a spreadsheet to calculate the laser power required for tritium separation by a photoreactor based on cylindrical waveguides. If cylindrical waveguides are to be considered again then this spreadsheet should be replaced or updated. In particular, the table of dissociation probabilities should be recalculated from either the SDT model or the CLND model.

A comparison of SEPCOST.WR1 with EQCELL.WR1 requires some care in defining the appropriate conditions. Given the need for updating parts of SEPCOST.WR1, it is probably better just to give a sample of the output for

conditions nominally the same as used for Table II, i.e. a gas pressure of 200 torr and a temperature of 198 K. The minimum critical fluence allowed by the present version of the spreadsheet is 40 J/cm^2, higher than the critical fluence used above. The other essential input parameter is the breakdown threshold of the gas, taken as 100 J/cm^2 for this example. The spreadsheet listing in Appendix G shows one solution obtained for these conditions. The total optical laser power required is 391 kW and the figure of merit P_f is 0.503 kW/mol/hr. These values place the cylindrical waveguide somewhere in the middle of Table II, as we would expect from an effective dissociation probability of about 0.15 (see Appendix G).

The number of photoreactors required for a satisfactory solution in SEPCOST.WR1 is fixed by the maximum allowed flow velocity for the specified diameter of waveguide. The repetition rate of the lasers is then fixed by the flow velocity, the length of the waveguide and the number of pulses each gas plug must encounter. In turn, the optimum dimensions of the cylindrical waveguides depend on the absorption coefficient of the gas.

This complex interdependency of the laser parameters, the dimensions of the photoreactors and the absorption in the gas is characteristic of all waveguide designs. It points out the need for a better understanding of the absorption properties of CF_3H before there can be much progress in photoreactor development.

7. LASER FOR PHOTOREACTORS

A fundamental assumption of photoreactor design so far is that the lasers required for the photoreactor are readily available. If we restrict our attention to pulsed CO_2 lasers then this is true for the most part; the technology of CO_2 lasers is highly advanced. (The only possible alternative to CO_2 lasers is free electron lasers, but they are still in a very early stage of development.) What is possible in the laser laboratory, however, may not always be practical, technically or economically, for a large-scale commercial application. Some of these concerns have been documented in a report to CFFTP by Dr. John Nilson in 1989. Here let us consider the parameters of pulsed CO_2 lasers that are important for photoreactor design: pulse duration, pulse energy, beam profile, and repetition rate. Note that wavelength is not in this list. The choice of wavelength is critical for dissociation, but photoreactor design for infrared multiphoton dissociation is practically independent of wavelength.

The first two parameters, pulse duration and energy, are closely related (see also Section 3). Table III lists the characteristic pulse lengths available and their methods of production. CO_2 lasers operate most efficiently by emitting a long pulse on the line 10P(20). The optimum wavelength for dissociation of CF_3T is closer to 9R(14) where the pulse energy, and hence the electrical efficiency, is slightly lower. By removing most of the nitrogen from the laser gas mixture, a shorter pulse is obtained again with a drop in efficiency. The shortest pulses require complex optics and an amplifier to boost the pulse energy, with a corresponding drop in efficiency. In general, CO_2 laser amplifiers are less efficient than oscillators; the amplified beam does not fill the discharge volume as much as the oscillator modes do. The maximum energy from a TEA CO_2 oscillator is about 10 J. For higher pulse energies an amplifier is essential. The maximum energy density available from CO_2 lasers is about 1 J/cm^2. Thus the maximum output energy of a CO_2 laser system is proportional to the area of the final amplifier.

Table III. CO_2 lasers for isotope separation.

Pulse Length	Electrical Efficiency	Method of Production
Long (1000 ns)	0.10	Energy transfer: N_2 to CO_2
	0.07	Peak output at 10P(20)
		Dissociation at 9R(14)
Medium (50-100 ns)	0.02	Energy stored in CO_2
		9R(14)
Short (1-10 ns)		Oscillator and amplifier
		Complex optics
	0.007	9R(14)

The spatial profile (transverse mode structure) of a beam from a laser oscillator is determined by the optical resonator. For long distance propagation and superior focusing characteristics, the preferred profile is the gaussian shape of the TEM_{00} mode, the lowest order transverse mode. A stable resonator will produce a gaussian beam if there is an aperture near one mirror. The disadvantage of this method is that the aperture reduces the maximum pulse energy. An unstable resonator will extract all the energy from a laser discharge in a beam that is nearly gaussian in the far field of the laser. The hard edges of most optics for unstable resonators produce unwanted diffraction rings in the near field. Now there are graded reflectivity mirrors, e.g. available from The National Institute of Optics associated with Laval University in Quebec, that provide a gaussian-like smooth spatial profile in the near field of an unstable resonator.

The longitudinal mode structure of a CO_2 laser oscillator affects the temporal profile of the output pulse. A smooth temporal profile in a long pulse is the sign of oscillation in a single longitudinal mode (SLM). (In a train of short pulses it is the sign of modelocking.) Most of the experiments mentioned in this report were performed with a laser operating in a single longitudinal mode. While SLM output simplifies the analysis of experiments, there is no obvious reason for using SLM output instead of multi-mode output.

Finally, the repetition rate of a CO_2 laser system affects the rate of gas processing in a photoreactor. We have seen in Section 6 that the minimum total optical power required for the 500 kg/hr plant is about 40 kW. This is average power, i.e. the product of energy per pulse and the repetition rate. Thus, a high repetition rate can compensate for a low pulse energy. The maximum repetition rate for a pulsed CO_2 laser is 1 kHz. Such lasers require rapid flow of the laser gas mixture for cooling and for catalytic recombination of dissociated CO_2. Conventional TEA CO_2 lasers can operate up to about 100 Hz. If short pulses are required then the electro-optic switch will probably limit the repetition rate to the order of 10 Hz or less.

Dr. John Nilson has investigated one other approach to lasers for photoreactors. He has analyzed the possibility of an intra-cavity photoreactor, a cell inside the laser resonator. This concept could be tested with our existing lasers and feasible optics. A 25% feedback from the cell to the laser would provide a fairly uniform fluence for measuring dissociation in a well-defined geometry. One disadvantage of this approach is the strong dependence of the design on the absorption in the cell, so that the design is not very flexible for investigating a range of conditions. A related concept, according to Dr. Nilson, is the long effective length resonator developed by Drs. Paul Corkum and Neil Burnett of the National Research Council of Canada. This resonator on an otherwise conventional CO_2 laser produces 2 or 3 short pulses in a span of 50 to 100 ns. It would be interesting to investigate dissociation with this type of pulse sequence.

For a commercial application of lasers the main concerns are cost and the long-term reliability of the laser system. From the considerations above, short-pulse lasers are poor in both areas mainly because of their complexity. Conventional TEA CO_2 oscillators are the simplest laser systems and have demonstrated reliable long-term operation. From Table III we see that these lasers can produce medium length pulses just by changing the laser gas mixture. The results in Section 3 demonstrate that medium length pulses are better than long pulses for dissociation. The limitation on average power from a single oscillator is not a serious concern. Although the laser power analyses in Section 6 treated the case of one laser per photoreactor, there is no fundamental reason why the input for one photoreactor could not be supplied by several lasers. Multiplexing in space and time might be easier than building one large laser with the equivalent average power output.

8. SUMMARY AND CONCLUSIONS

The problem of photoreactor design is still an active area for investigation and development. Given the present state of knowledge as reviewed in this report, there is no single path to follow for the optimum development of a prototype photoreactor. On the other hand, the research to date provides several guidelines that limit the design possibilities.

An important development in this report is the figure of merit provided in Section 2. The expression for P_D in Eq. 3 contains all the essential parameters required to evaluate different laser and photoreactor combinations. In

particular, P_D specifically includes the effect of the type of gas flow through the photoreactor. The cost of dissociation determined by P_D could be incorporated in a flowsheet of the complete process to estimate the total cost of laser-based tritium separation.

The necessary conditions for efficient dissociation are fairly well known. The gas temperature must be less than -50°C and the gas pressure may range up to 200 torr. The fluence for dissociation depends on the pulse length of the laser beam. The choice of pulse length may depend on the material properties of the windows and mirrors, as well as on the cost and reliability of the laser method to produce the pulses.

Precise knowledge of the absorption of CO_2 laser energy in CF_3H is vital to the design of any photoreactor. Unfortunately, this fundamental property is not known very well for some of the conditions of interest for dissociation. In particular, the pressure dependence of absorption in CF_3H should be measured as a function of pulse length and fluence.

Some specific photoreactor designs have been developed. The equifluence cell design is not very realistic in its treatment of beam propagation, but it is useful for assessing the theoretical minimum laser power required for a given application. Beam confinement, either by focusing or waveguiding or both, is needed to provide the long path lengths for efficient utilization of the laser energy. The cylindrical waveguide has been demonstrated on a very small scale. Its major disadvantage for large-scale applications is the limited flow rate it can accommodate. Continued research may yet find a way to improve the gas flow in this design. The parallel-plate waveguide described in this report is an attempt to combine high gas flow with confinement of the laser beam. Because of its multipass geometry, the parallel-plate waveguide is also more compact than the cylindrical waveguide. A working model of the parallel-plate photoreactor would be a useful testing ground for many aspects of photoreactor design, e.g. absorption in CF_3H and longevity of internal mirrors.

The spreadsheet programs described in this report should be considered as tools to help design photoreactors. They are not the final word in evaluating the costs of LIS for tritium separation. It is very difficult to estimate the cost of the lasers for a large-scale application mainly because no one has ever built such a system. As Ontario Hydro continues to develop laser-based tritium separation it will be leading the rest of the world in the demonstration of a facility for isotope separation based on infrared multiphoton dissociation.

ACKNOWLEDGEMENTS

As consultant to the LIS project, Dr. John Nilson provided encouragement and advice, both gratefully received. I am pleased to thank Dr. Kazuo Takeuchi and his staff at The Institute for Physical and Chemical Research (RIKEN) in Japan for providing the time and facilities to allow me to finish this report during my tenure as an STA Fellow there.

Approved:

A.F. Baljet
Manager
Electrical Research Department

Submitted:

Hugh D. Morrison*
Physicist
Science Section

*Dr. H.D. Morrison is on an 18-month Attachment at RIKIN, Japan.

REFERENCES

1. J.C. Vanderleeden, "Depletion optimization and photon efficiency in laser isotope separation of deuterium," Appl. Opt. **17**, 785-796 (1978).

2. J.A. O'Neill, "Multiphoton dissociation experiments in capillary waveguide cells," in *Conference on Lasers and Electro-Optics Technical Digest* (Optical Society of America, Washington, DC 1984), pp. 168-170.

3. F.E. Bartoszek, K.E. Donnelly, K.M. Kalyanam, H.D. Morrison, J.A. O'Neill, J.R. Robins, S.K. Sood, K.B. Woodall, and O.K. Kveton, "Laser-based hydrogen isotope separation system for large-scale applications," *Fusion Technology 1988*, A.M. Van Ingen, A. Nijsen-Vis, H.T. Klippel, Editors (Elsevier Science Publishers B.V. 1989) pp. 1317-1321.

4. J.B. Marling, I.P. Herman and S.J. Thomas, "Deuterium separation at high pressure by nanosecond CO_2 laser multiple-photon dissociation," J. Chem. Phys. 72, 5603-5634 (1980).

5. I.P. Herman, K. Takeuchi, and Y. Makide, "Laser Separation of Tritium," *Laser Applications in Physical Chemistry*, D. Keith Evans, ed. (Marcel Dekker 1989), pp. 173-220, and references therein.

6. Y. Makide, S. Hagiwara, T. Tominaga, K. Takeuchi, and R. Nakane, "Tritium isotope separation by CO_2 laser-induced multiphoton dissociation of CTF_3," Chem. Phys. Lett. **82**, 18-24 (1981).

7. K. Takeuchi, S. Satooka, and Y. Makide, "Tritium isotope separation by CO_2-laser irradiation at low temperatures," Appl. Phys. **B33**, 83-90 (1984).

8. F. Magnotta and I.P. Herman, "Observations on the spectral dependence and T/D isotopic selectivity in the CO_2 laser multiple-photon dissociation of trifluoromethane," Appl. Phys. **B36**, 207-212 (1985).

9. K. Takeuchi and I. Inoue, "Optimum irradiation geometry in continuous laser isotope separation," J. Chem. Eng. Japan **19**, 81-83 (1986).

10. K. Takeuchi and S. Satooka, "Efficient Energy Utilization in Laser-Assisted Isotope Separation of Tritium," J. Nucl. Sci. Technol. **25**, 489-494 (1988).

11. H.D. Morrison, "Pulse length dependence of trifluoromethane-t dissociation," *Digest of Technical Papers*, Tenth Annual Meeting of the Laser Society of Japan (1990), pp. 102.

12. E. Suzuki, S. Kato, and K. Takeuchi, "Accurate extraction of reaction probabilities in IR multiphoton dissociation by a focused Gaussian beam: an improved analytical method," Appl. Opt. 27, 4445-4449 (1988).

13. K. Takeuchi and S. Satooka, "Optimization in CO_2-laser isotope separation of tritium," *Laser Applications in Chemistry*, D. Keith Evans, Editor, Proc. SPIE 669 (1986), pp. 18-20.

14. Measurements performed by Janice Cheung, a summer student in 1989, with a cw CO_2 laser borrowed from the Laser Facility at the University of Toronto.

15. H.D. Morrison, "Mode Matching a CO_2 Laser Beam to a Waveguide," Research Report E87-23-K.

16. D.W. Lupo and M. Quack, "Quantitative infrared photochemistry at high energy densities: $CFCl_3 \rightarrow CFCl_2 + Cl$," Chem. Phys. Lett. **130**, 371-376 (1986).

17. K. Takeuchi, M. Motoyama, and I. Inoue, "Three-compartment photoreactor for laser isotope separation of tritium," Sep. Sci. Technol. 22, 95-102 (1987).

18. "CRC Standard Mathematical Tables," 21st ed. (The Chemical Rubber Company, 1973), pp. 582-583.

19. W.H. Press, B.P. Flannery, S.A. Teukolsky, and W.T. Vetterling, "Numerical Recipes: The Art of Scientific Computing," (Cambridge University Press, 1986), pp. 163-164.

20. A.E. Siegman, "Lasers," (University Science Books, 1986), pp. 697.

21. S. Nemoto, "Determination of Waist Parameters of a Gaussian Beam", Appl. Opt. 25, 3859-3863 (1986). Also summarized in Appendix B of Research Report E87-23-K. There are some typographical errors in the equations listed in E87-23K, so check with the original paper.

22. J.J. Degnan, "The Waveguide Laser: A Review," Appl. Phys. 11, 1-33 (1976).

23. A.E. Siegman, "Lasers," (University Science Books, 1986), pp. 734.

24. H. Nishihara, T. Inoue, and J. Koyama, "Low-loss parallel-plate waveguide at 10.6 μm," Appl. Phys. Lett. 25, 391-393 (1974).

25. R.A. Mail, F.J. Markovich, and R.H. Carr, "Cost analysis of Lasers for a Laser Isotope Separation System, Final Report," UCRL-13744-2 (1977) General Research Corporation, Energy Research and Development Administration, Santa Barbara, CA.

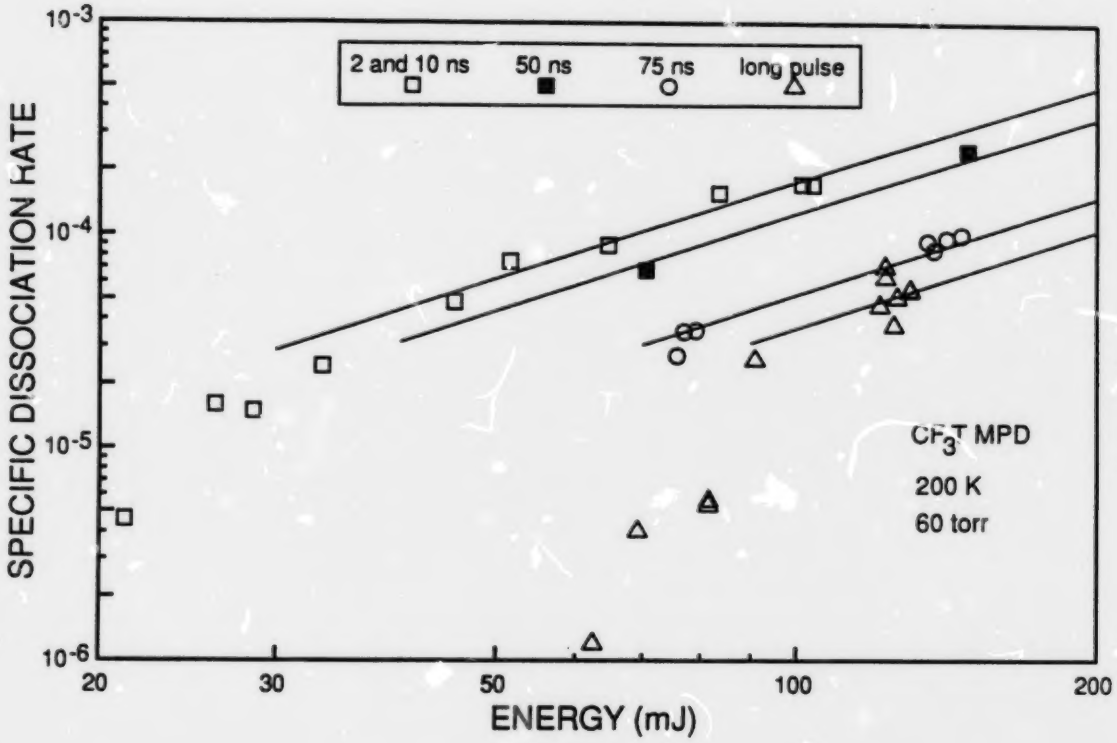

Figure 1: Specific dissociation rate as a function of pulse energy and pulse length for CF_3T irradiated with CO_2 laser line 9R(14). The lines have a slope of 3/2 on this log-log graph, demonstrating the 3/2-power dependence of the dissociation at high energies.

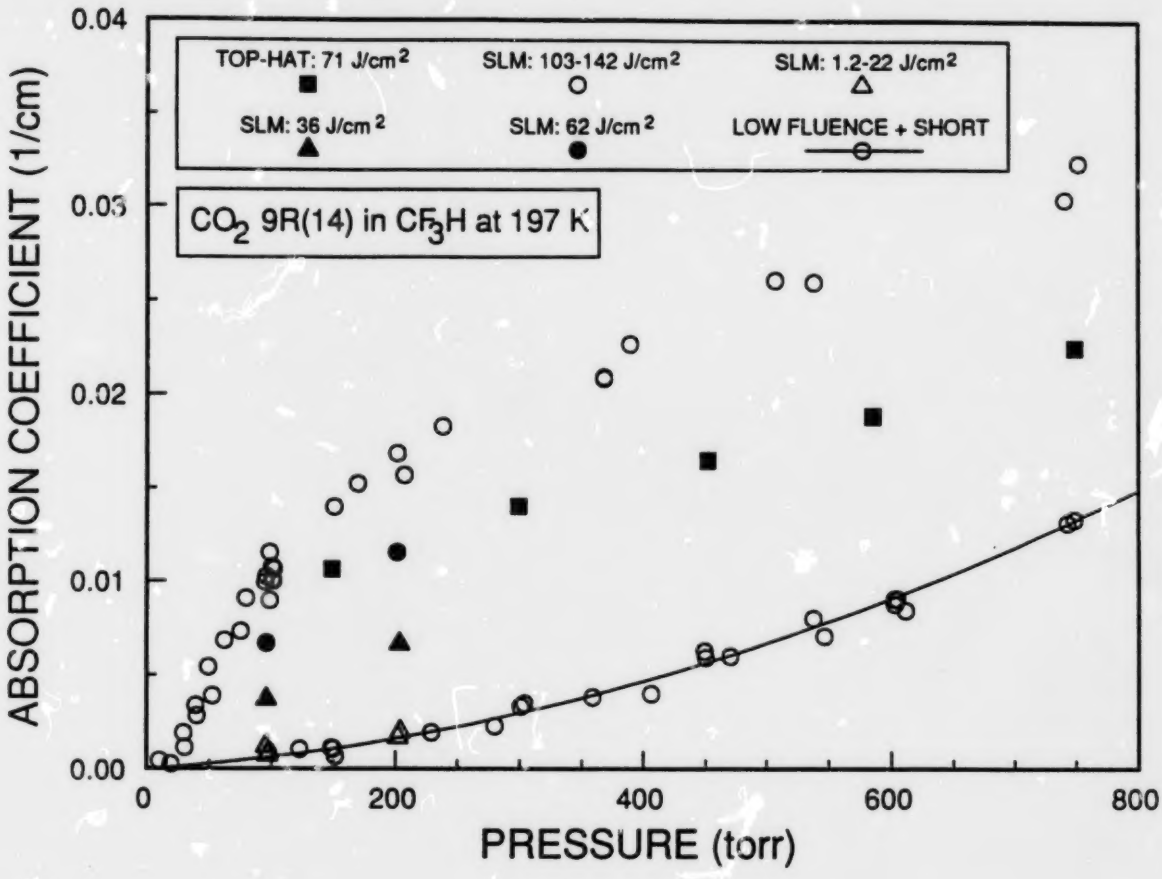

Figure 2: Absorption of CO_2 laser line 9R(14) in CF_3H as a function of pressure and of peak fluence in the laser beam. The cell length was 56 cm. For all cases the laser was operating in a single longitudinal mode (SLM) with a gaussian cross-section. The "top-hat" beam was produced by passing the central portion of the gaussian beam through a 12-mm diameter aperture. All pulses were 1 μs long except for some 2-ns and 10-ns pulses indicated as "short" in the legend. The solid curve is a least-squares fit through the origin for the small-signal absorption.

APPENDIX A

POSTER PAPER

This poster was presented at The Institute for Physical and Chemical Research (RIKEN), Wako-shi, Saitama, Japan, at their Symposium on Laser Science, 17-18 January 1990.

A.1 SUMMARY

PHOTOREACTOR DESIGN FOR LASER-BASED TRITIUM SEPARATION

H.D. Morrison

Ontario Hydro Research Division
800 Kipling Ave., KR143
Toronto, Ontario
Canada M8Z 5S4

The application of multiphoton dissociation (MPD) of molecules to laser isotope separation (LIS) has been studied for many years. Many molecule and laser combinations have successfully demonstrated the separation of isotopes, especially isotopes of hydrogen and carbon. One of the fundamental problems that remains to be solved before commercial development of LIS can proceed is the design of efficient photoreactors. Any photoreactor must provide the required enrichment in the product stream while achieving the required level of depletion in the feed stream. Efficiency has two meanings in this case. Firstly it implies the photon utilization efficiency, meaning the fraction of photons entering the photoreactor that are actually absorbed by molecules and cause dissociation. Secondly it implies the dissociation efficiency, meaning the fraction of the photoreactor volume where complete dissociation of the target molecule occurs. The design of an efficient photoreactor depends on the specific application because every molecule is different in terms of photon absorption, optical selectivity, critical fluence for dissociation, temperature and pressure dependence of dissociation, and chemical reactivity.

At Ontario Hydro we are working on scaling up a process to separate T from H based on MPD of trifluoromethane, CF_3T in CF_3H. This process requires a fluence on the order of 10-60 J/cm², depending on the CO_2 laser pulse length. As this fluence exceeds the damage threshold for all window materials we must allow for beam compression inside the photoreactor to reach the critical fluence for dissociation. To achieve high photon utilization requires a path length of several meters, but this must be combined with refocusing to maintain a fluence greater than the critical fluence for dissociation and achieve high dissociation efficiency.

Several photoreactor designs have been proposed for MPD of trifluoromethane.[1-3] We propose a multipass cell between parallel plates based on the propagation of a gaussian beam. The choice of a gaussian beam not only simplifies modelling of the process but also provides a consistent fluence distribution in the photoreactor. The multipass geometry provides a long absorption path length in a compact structure. The parallel plates maintain gas flow transverse to the direction of beam propagation, thus intercepting the beam without impeding gas flow. Internal mirrors of diamond-turned copper will refocus the beam on every pass to maintain a high fluence. The focal lengths of the mirrors are determined by the beam absorption losses. As the beam is a single mode, it must be mode-matched from the laser into the photoreactor. A telescope after the entrance window achieves this task as it compresses the beam to the critical fluence for dissociation. Good beam control also requires that all apertures be large enough to minimize ripples in the beam intensity profile. Ripples of less than 1% require aperture diameters at least 4.6 times the beam radius, where radius is defined as $1/e^2$ in intensity. One possibility, however, for reducing the volume where the fluence is too low for dissociation to occur is to place the parallel plates close enough to act as a waveguide in one dimension. In this case the focusing mirrors are still required to compress the beam in the other dimension. Calculations will be presented for both geometries to estimate the efficiency of this design.

Even this design will not be sufficient to achieve the ideal of one pulse per molecule where high levels of depletion are required. An analysis of product enrichment and feed depletion yields simple expressions in terms of the average dissociation per pulse and the number of pulses for two cases of gas mixing after each pulse: totally mixed and totally unmixed. Conceptually, the analysis is similar to the laser separation reactor of Vetsko et al.,[4] although the results are quite different in the regime of a few pulses, less than 10. Calculation of the feed depletion as a function of the dissociation per pulse provides a target of 60% dissociation per pulse to achieve 90% depletion in 6 pulses for the mixed feed stream. If a gradient of depleted feed can be maintained by not mixing the gas then only 2.5 pulses are required. Careful control of the gas flow through the photoreactor will achieve tremendous savings in laser energy for this process and any other MPD process.

1. J.C. Vanderleeden, "Depletion optimization and photon efficiency in laser isotope separation of deuterium," Appl. Opt. 17, 785-796 (1978).

2. J.A. O'Neill, "Multiphoton dissociation experiments in capillary waveguide cells," in *Conference on Lasers and Electro-Optics Technical Digest* (Optical Society of America, Washington, DC 1984), pp. 168-170.

3. K. Takeuchi, M. Motoyama, and I. Inoue, "Three-Compartment Photoreactor for Laser Isotope Separation of Tritium," Separation Science and Technology 22, 95-102 (1987).

4. V.M. Vetsko, O.A. Devdariani, S.A. Kalitin, V.A. Kaminskii, N.I. Laguntsov, and G.A. Sulaberidze, "Cascading of laser isotope separation cells," Sov. J. Quantum Electron. 15, 827-831 (1985).

A.2. POSTER SLIDES

SLIDE 1:

PHOTOREACTOR DESIGN
FOR LASER-BASED
TRITIUM SEPARATION

Hugh D. Morrison
Ontario Hydro Research Division
Toronto, Ontario, Canada

SLIDE 2:

HIGH EFFICIENCY REQUIRED

- Photon utilization Efficiency
  - fraction of photons absorbed
  - requires a long path length
- Dissociation Efficiency
  - fraction of photoreactor volume where complete dissociation occurs
- Design depends on specific application

SLIDE 3:

TRITIUM LIS AT ONTARIO HYDRO

- Based on MPD of CF_3T in CF_3H
- Fluence for dissociation: 10 to 60 J/cm^2
  - exceeds damage threshold for windows
  - requires beam compression inside the photoreactor
- Absorption path length (1/e): 10 to 50 m
  - requires refocusing
    or
    beam confinement (waveguide)

SLIDE 4:

PARALLEL-PLATE GEOMETRY

- Multipass - long path in compact cell
- Gas flow transverse to laser beam
  - high flow rates possible
- Gaussian beam input: radius w
  - good mode control for refocusing
- Plate separation: 2a
  - open cell for (w/a)<0.44
  - waveguide for (w/a)=0.77

SLIDE 5:

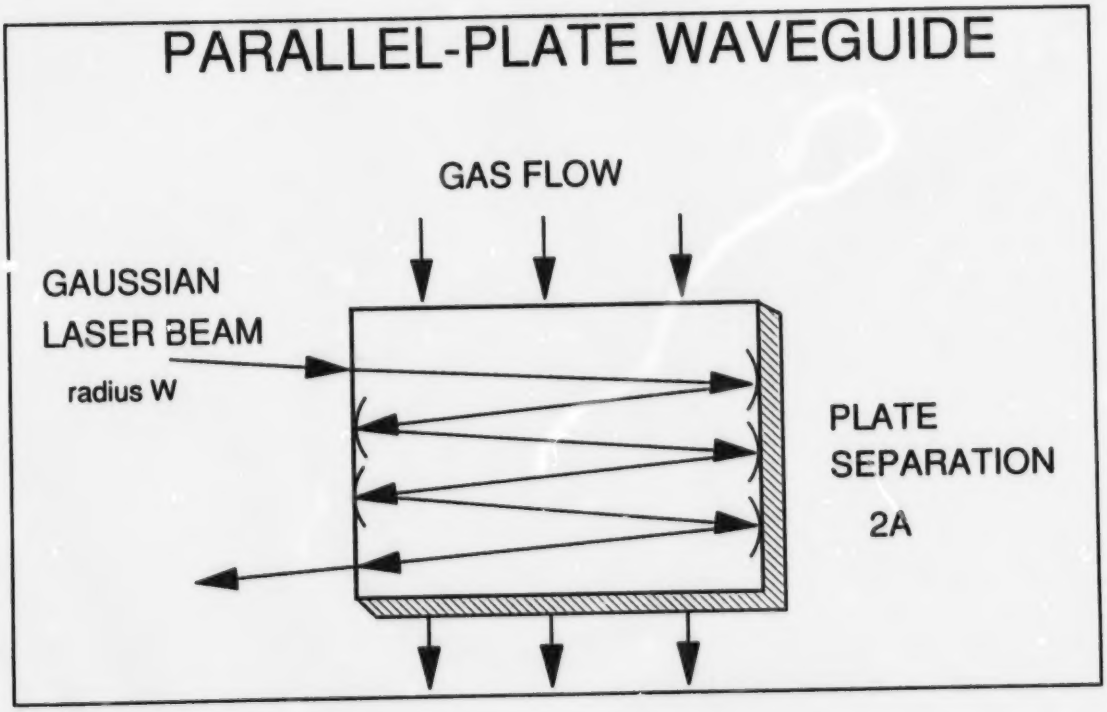
PARALLEL-PLATE WAVEGUIDE
GAS FLOW
GAUSSIAN
LASER BEAM
radius W
PLATE
SEPARATION
2A

SLIDE 6:

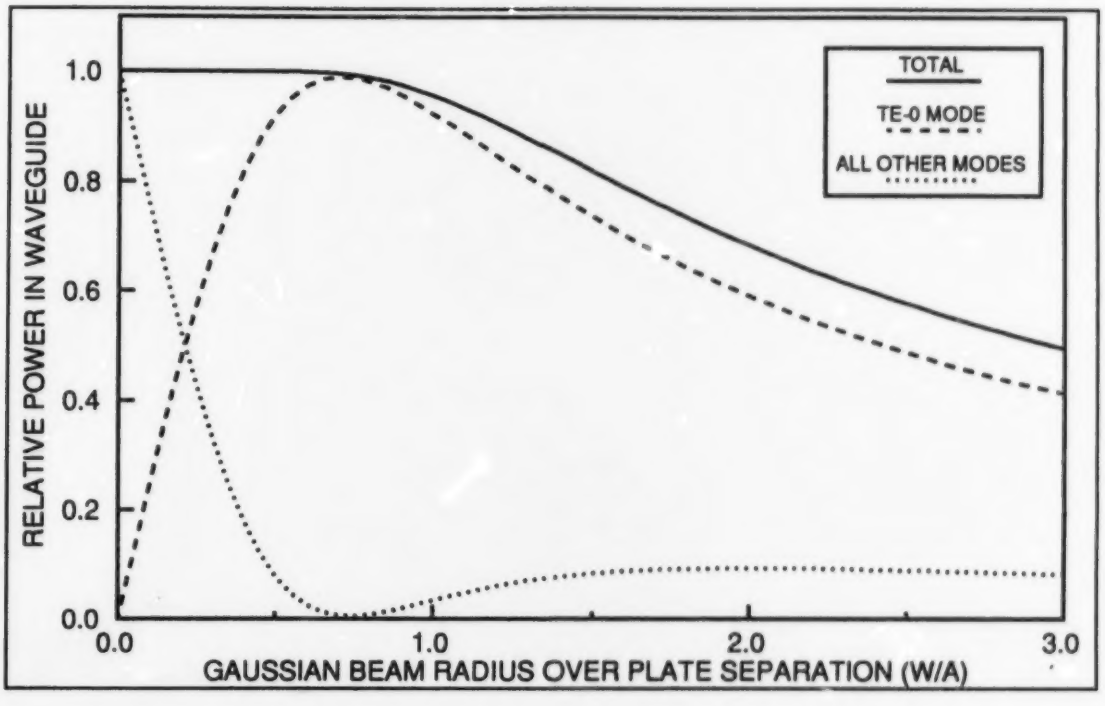
TOTAL
TE-0 MODE
ALL OTHER MODES
RELATIVE POWER IN WAVEGUIDE
1.0
0.8
0.6
0.4
0.2
0.0
0.0
1.0
2.0
3.0
GAUSSIAN BEAM RADIUS OVER PLATE SEPARATION (W/A)

SLIDE 7:

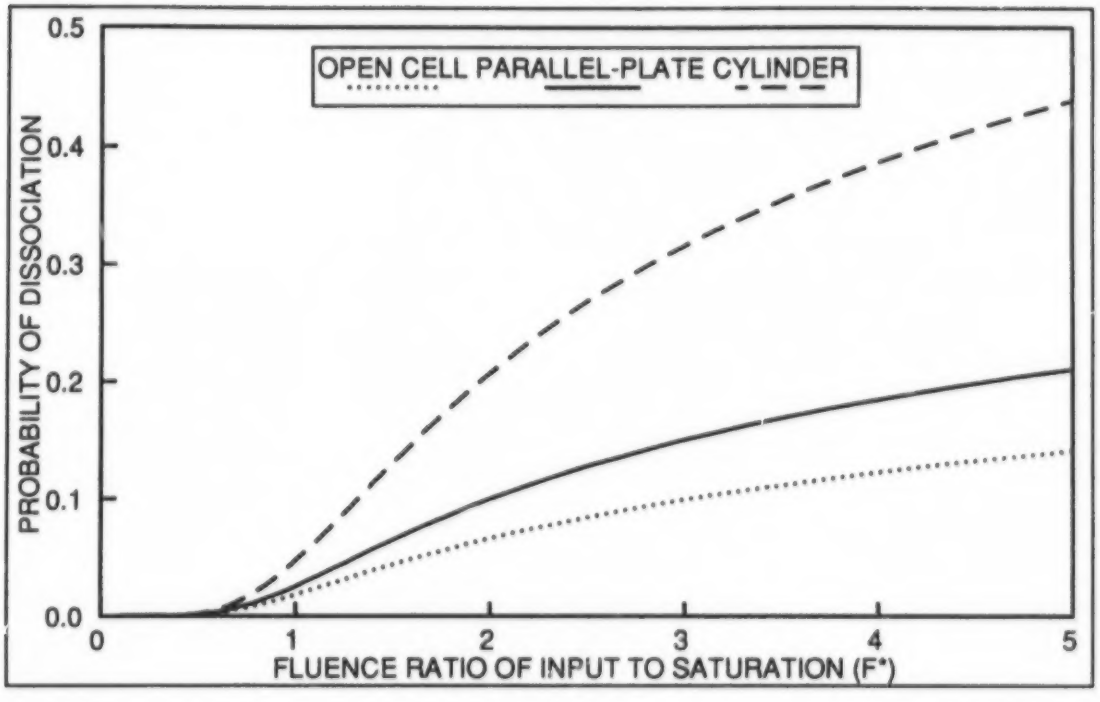

SLIDE 8:

MEASURE OF EFFICIENCY
FIGURE OF MERIT

- amount of feed processed per laser power

- laser power is proportional to 'n'

SLIDE 9:

EFFECT OF MIXING ON DEPLETION

- Definitions:
  - Q: Required depletion
  - q: Dissociation probability per pulse
  - n: Number of pulses to achieve Q

- Unmixed (plug flow):

$$n = \ln (1-Q) / \ln (1-q)$$

- Mixed (turbulent flow):

$$n = [\, Q (1-q)] / [(1-Q)\, q\,]$$

SLIDE 10:

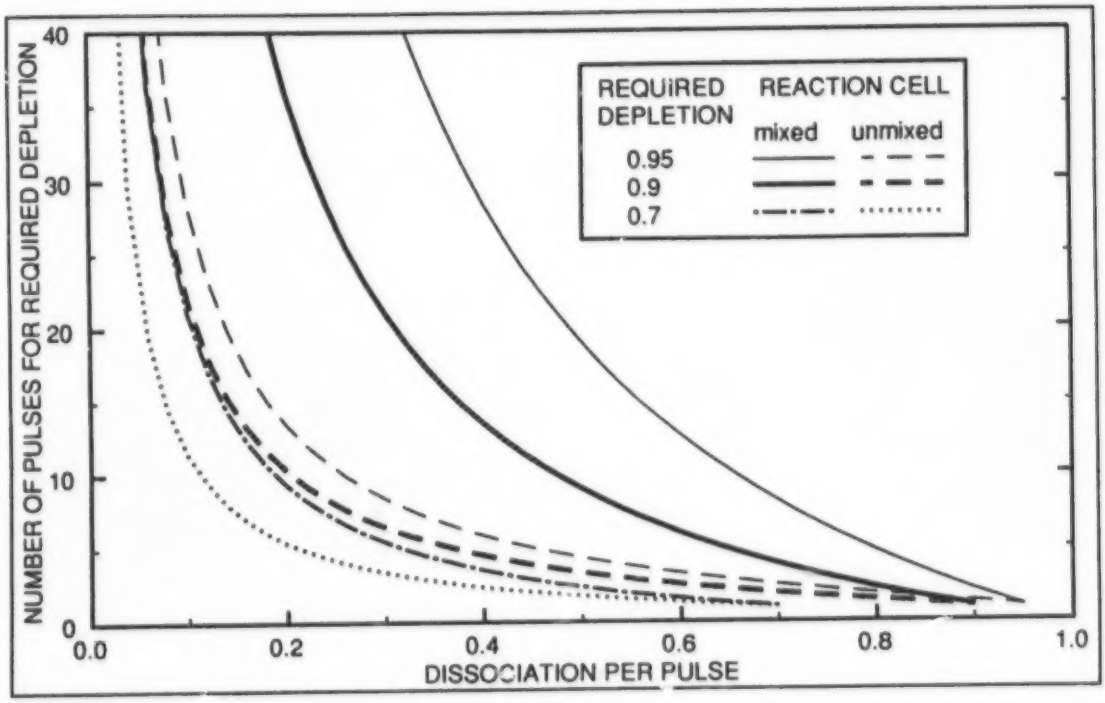

SLIDE 11:

CONCLUSIONS

PARALLEL-PLATE CELL IS FEASIBLE

- Gaussian beam couples efficiently into 1 mode

- Dissociation efficiency
  - 50% better than open cell
  - 50% as good as cylinder

- Gas flow superior to cylinder

APPENDIX B

DEPLETION IN A PHOTOREACTOR: PLUG FLOW AND STIRRED FLOW

The depletion (Q) achieved in a photoreactor depends on the average residence time (t) of gas in the photoreactor and on the effective fraction of dissociation per pulse (ε_v). The fundamental formula for the average fraction of dissociation per pulse in a photoreactor is

$$b = (1/V) \int_v q(\Phi)\, dV , \tag{B.1}$$

where $q(\Phi)$ is the fluence dependent probability of dissociation and V is the interaction volume. The application of this formula depends on the type of gas flow through the photoreactor. Plug flow and stirred flow are the two extremes of gas flow.

B.1 PLUG FLOW

Follow one plug of gas as it flows through the photoreactor. For each pulse of the laser the gas plug is in a different location with a corresponding average fraction of dissociation (b_j). Calculate the relative fractions of T in the target molecule CF_3T and in the product molecule TF for each of the t pulses.

Pulse Number	Fraction of T as TF	Fraction of T as CF_3T	
0	0	1	(B.2a)
1	$b_1 \cdot 1$	$1-b_1$	(B.2b)
2	$b_1 + b_2(1-b_1)$ $= 1 - (1-b_1)(1-b_2)$	$(1-b_1)(1-b_2)$	(B.2c)
3	$1 - (1-b_1)(1-b_2)$ $+ b_3(1-b_1)(1-b_2)$ $= 1 - (1-b_1)(1-b_2)(1-b_3)$	$(1-b_1)(1-b_2)(1-b_3)$	(B.2d)
.	.	.	
.	.	.	
.	.	.	
t	$1 - \prod_{j=1}^{t}(1-b_j)$	$\prod_{j=1}^{t}(1-b_j)$	(B.2e)

If we now define the effective probability of dissociation per pulse ε_v by

$$(1-\varepsilon_v)^t \equiv \prod_{j=1}^{t}(1-b_j) \tag{B.3}$$

then the fraction of CF_3T remaining, 1–Q, is given by

$$1-Q = (1-\varepsilon_v)^t . \tag{B.4}$$

Solving for t we get

$$t = \ln (1-Q) / \ln (1-\varepsilon_v) . \tag{B.5}$$

B.2 STIRRED FLOW

In this case we must consider the entire volume of gas in the photoreactor at once, and follow the change in concentration of CF_3T from one pulse to the next. Therefore, the effective probability of dissociation per pulse is just the fraction of dissociation per pulse for the whole photoreactor, i.e. $\epsilon_v = b$. In the steady state, the concentration of CF_3T and of the other components measured at any given point in the pulse cycle is unchanged from pulse to pulse. As the average residence time of a molecule is t pulses, we must remove a fraction V/t of the gas after each pulse and replace it with fresh gas. Just before the pulse the fraction of T as TF is x and the fraction of T as CF_3T is 1–x. Just after the pulse the fraction of T as TF is $x+\epsilon_v(1-x)$, thus the fraction of T as CF_3T is $(1-\epsilon_v)(1-x)$. A fraction of this gas is removed as the product stream. Therefore the concentration of CF_3T remaining in the product stream, 1–Q, is just

$$1-Q = (1-\epsilon_v)(1-x) . \tag{B.6}$$

To calculate x, or 1–x, we must consider the gas concentrations in the photoreactor after adding fresh gas and stirring the mixture. Note that we have made the simplifying assumption that none of the fresh gas leaves the photoreactor before the next pulse. The new mixture contains 1–1/t parts of $(1-\epsilon_v)(1-x)$ and 1/t parts of 1, i.e. the fresh gas contains no TF. The concentration of the new mixture is 1–x by definition. Thus we have

$$1-x = (1-1/t)(1-\epsilon_v)(1-x) + 1/t . \tag{B.7}$$

Solving Eq. B.7 for 1–x yields

$$1-x = 1/[\epsilon_v(t-1)+1] . \tag{B.8}$$

Substitution this expression for 1–x into Eq. B.6 and solving for t gives

$$t = Q(1-\epsilon_v) / [\epsilon_v(1-Q)] . \tag{B.9}$$

APPENDIX C

MODELS FOR PROBABILITY OF DISSOCIATION

The analysis of experiments in pulsed infrared multiphoton dissociation (IRMPD) requires a theoretical model based on the fluence distribution, $\Phi(x,y,z)$, in the photoreactor and on the dissociation probability, $q(\Phi)$, per pulse. The integral of the dissociation probability over the cell volume, V_c, yields the reaction volume, V_R, which is the effective volume where complete dissociation occurs:

$$V_R = \int q dV \, . \tag{C.1}$$

The reaction volume defines the experimentally measured dissociation rate, b, by

$$b \equiv V_R/V_c = -(1/t) \ln (1-Q) \, , \tag{C.2}$$

where t is the number of pulses and Q is the dissociated fraction (depletion) of the reactant molecule.

The most elementary model for q is the simple dissociation threshold (SDT), used for most of the cost estimating models to date. In the SDT model there is a threshold for dissociation labelled as the critical fluence for dissociation, Φ_c. Where the local fluence is greater than or equal to Φ_c the dissociation probability is 1. Where the local fluence is less than Φ_c no dissociation occurs. Thus, the calculation of V_R reduces to finding the volume where the fluence is not less than Φ_c.

Reference 12 surveys several more complex models for the dissociation probability and then discusses the Cumulative Log Normal Distribution (CLND) applied to a focused gaussian beam. They have found that the CLND model provides the best fit to experimental results in the regime near Φ_c of the SDT model, as well as at lower and higher fluences. There are two parameters in the CLND model: the saturation fluence, Φ_s, corresponding to the fluence where q is 0.5, and the width parameter, σ, corresponding to the standard deviation of the normal distribution. The expression for q is an integral:

$$q = 1/[(\sigma(2\pi)^{1/2}] \int_{-\infty}^{\Phi} \exp [-(\ln \Phi - \ln \Phi_s)^2/(2\sigma^2)] \, d \ln \Phi \, . \tag{C.3}$$

If we let

$$x = (\ln \Phi - \ln \Phi_s) / \sigma \tag{C.4}$$

then

$$q = F(x) = 1 - (1/2) \cdot \mathrm{erfc} \, (x/\sqrt{2}) \tag{C.5}$$

where F is the cumulative normal distibution function and erfc is the complementary error function.[18] A convenient numerical routine for calculating erfc is listed in Ref. 19.

It is possible to relate the parameters of the CLND model to a simpler model as described by Suzuki et al.[12] Thus, Φ_s can be obtained from dissociation at high fluence, and σ can be obtained from measurements at fluences less than Φ_s. For the conditions appropriate to our measurements of CF_3T dissociation, results by Takeuchi's group show that σ lies between 0.4 and 0.6 (Ref. 13). From this estimate of σ we can re-interpret our measurements of Φ_c in terms of Φ_s. Figure C.1 compares the SDT model with the CLND model on the basis of the peak fluence of a gaussian beam and Φ_c and Φ_s. In an experiment we measure the peak fluence and calculate Φ_c. The dimensionless ratio (F) of these two fluences is the ordinate in Fig. C.1; the abscissa is the ratio (F^*/F) of Φ_c to Φ_s, where F^* is the ratio of the peak fluence to Φ_s. Several curves show F^*/F as a function of F for a range of values of σ. All the curves show that F^*/F is nearly constant for F greater than 2. Thus, for a reliable measurement of Φ_c and then an estimate of Φ_s, the peak fluence in the experiment must be greater than twice Φ_c. For σ of 0.4 and 0.6, the average values of F^*/F, calculated for F between 2 and 5, are

0.894±0.005 (mean ± one standard deviation) and 0.773±0.012, respectively. These are the factors by which Φ_e underestimates Φ_s for these values of σ.

The CLND model can provide a quick estimate of the peak fluence required in a photoreactor to achieve a desired probability of dissociation. Recall that Φ_s is defined as the fluence where q is 0.5. In general, higher q values are desirable. Table C.I lists F*, the ratio of the peak fluence to Φ_s, calculated for a gaussian beam as a function of σ and q. As a rule of thumb, a peak fluence equal to twice the saturation fluence will provide a dissociation probability of 0.9, for the conditions appropriate to dissociation of CF_3T.

Table C.I

Ratio of peak fluence to saturation fluence in the CLND model calculated for a gaussian beam as a function of σ and q, the probability of dissociation.

q	F* = Φ / Φ_s		
	σ = 0.4	0.5	0.6
0.5	1.0	1.0	1.0
0.8	1.40	1.52	1.66
0.9	1.67	1.90	2.12
0.95	1.93	2.28	2.68
0.99	2.54	3.20	4.04

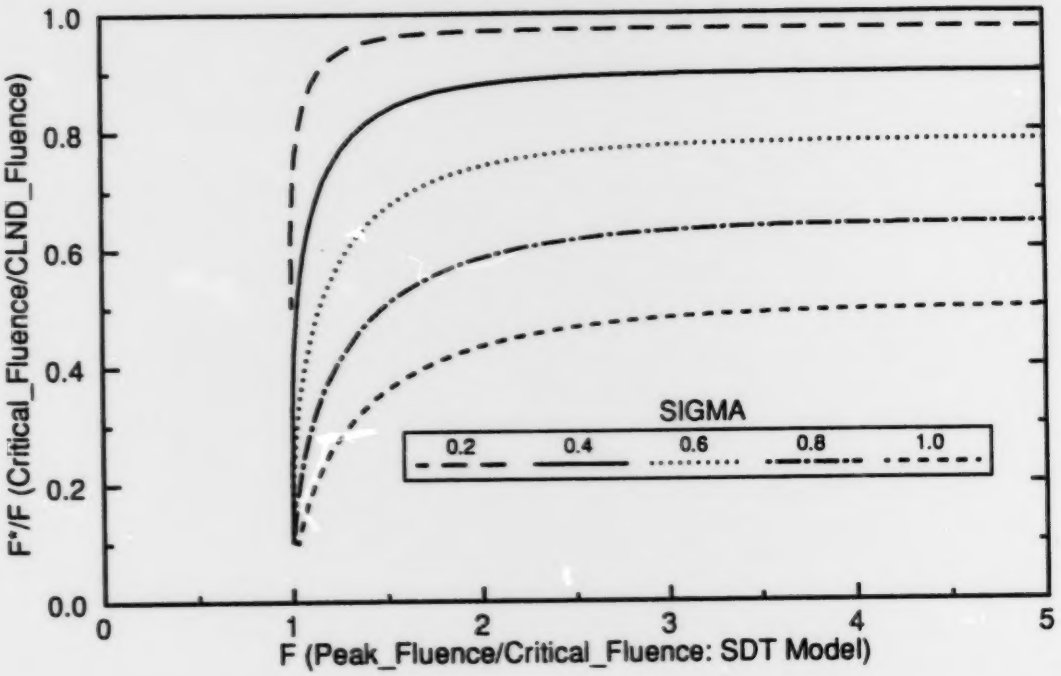

Figure C.1: A comparison of the SDT and CLND dissociation models for a focused gaussian beam neglecting absorption losses. F is the ratio of the peak fluence in the beam to Φ_C, the critical fluence for dissociation in the SDT model. F* is the ratio of the peak fluence to Φ_S, the saturation fluence in the CLND model, and σ (sigma) is the standard deviation of the log-normal distribution. The ratio F*/F as a function of F and σ provides a simple way of estimating Φ_S from a single-point calculation of Φ_C and an estimated range for σ.

APPENDIX D

GAUSSIAN BEAMS: PROPAGATION IN FREE SPACE AND COUPLING INTO WAVEGUIDES

D.1 GAUSSIAN BEAMS IN FREE SPACE

Refer to Research Report E87-23-K, "Mode Matching a CO_2 Laser Beam to a Waveguide", for a general summary of gaussian beams and the theory of their propagation. Here a gaussian beam has the form

$$\Phi(r,z) = \Phi(0,z)\ \exp[-2r^2/\omega^2(z)] \tag{D.1}$$

where $\Phi(0,z)$ is the on-axis peak fluence and $\omega(z)$ is the beam radius defined by

$$\omega^2(z) = \omega_f^2\ (1 + z^2/a^2)\ . \tag{D.2}$$

The peak fluence can be written as the product of the initial fluence and an exponential attenuation factor,

$$\Phi(0,z) = \Phi(0,0)\ \exp(-\alpha z)\ , \tag{D.3}$$

where α is the attenuation coefficient per unit length. The beam radius at the focus is ω_f and "a" is the Rayleigh range defined by

$$a = \pi\omega_f^2/\lambda \tag{D.4}$$

where λ is the wavelength. If the beam contains some higher order modes in addition to the lowest order TEM_{00} gaussian mode then the beam is characterized as being "N times diffraction limited", or NTDL.[20] If the TEM_{00} mode has a focal spot radius of ω_f then the NTDL beam has a focal spot of $\omega_N = N\cdot\omega_f$. Surprisingly, the Rayleigh range of the NTDL beam is identical to that of the TEM_{00} beam of spot size ω_f;

$$\begin{aligned} a_N &= \pi\omega_N^2/(\lambda N^2) \\ &= \pi N^2\omega_f^2/(\lambda N^2) \\ &= a\ . \end{aligned} \tag{D.5}$$

The equations of Nemoto (Ref. 21) have been extended to NTDL beams for the calculation of beam propagation in multi-pass cells. In this application, we fix the fluence at the ends of each pass and calculate the beam size at each end from the beam energy there, attenuated appropriately from the initial energy. To calculate the beam parameters (beam waist ω_0, and waist location z_0) for a TEM_{00} beam from the beam size at two positions (ω_1 and ω_2), Nemoto's equations apply directly. Numerically the only difference in Nemoto's equations to handle NTDL beams is the formula for the parameter r. Instead of

$$r = [\lambda(z_1-z_2)\ /\ (\pi\omega_1\omega_2)]^2\ , \tag{D.6}$$

simply use

$$r = [\lambda(z_1-z_2)N^2\ /\ (\pi\omega_1\omega_2)]^2 \tag{D.7}$$

in the formulas for the beam size and location. This has the same effect as letting the two NTDL beam sizes be ω_{1N} and ω_{2N} and defining $\omega_1=\omega_{1N}/N$ and $\omega_2=\omega_{2N}/N$ to calculate ω_0, z_0 and the Rayleigh range as before. Then for the NTDL beam, the waist location and Rayleigh range are unchanged, but the beam waist is $\omega_N=N\omega_0$.

D.2 COUPLING A GAUSSIAN BEAM INTO A WAVEGUIDE

Expressions for the field components and propagation constants of several types of waveguide are described in Ref. 22. Two types of waveguide are of interest here: a hollow dielectric cylinder, and a metal hollow-slab or parallel-plate. The lowest loss modes of propagation in these two waveguides couple efficiently to gaussian beams, and they are linearly polarized. In the hollow dielectric cylinder they are the hybrid EH_{1m} modes, and in the metal parallel-plate waveguide they are the transverse electric TE_m modes. We can express the electric field of an input gaussian beam as a sum over waveguide modes and then use the orthogonality property of the modes to evaluate the mode coupling coefficients. Let us first review the expressions for electric field, fluence and energy in a linearly polarized gaussian beam. The magnitude of the electric field can be written as

$$E_G = E_0 \exp(-r^2/\omega^2) , \tag{D.8a}$$

$$= E_0 \exp(-x^2/\omega^2) \exp(-y^2/\omega^2) , \tag{D.8b}$$

and then the fluence is just

$$\Phi_G \equiv (E_G)^2 = E_0^2 \exp(-2r^2/\omega^2) . \tag{D.9}$$

The total energy in the beam is found by integrating Φ_G over the x-y plane:

$$\text{Energy}_G = (\pi\omega^2/2)\, E_0^2 . \tag{D.10}$$

The energy passed by a circular aperture of radius "a" centered on the gaussian beam is given by

$$\text{Energy}_{circ} = (\pi\omega^2/2)\, E_0^2\, [1 - \exp(-2a^2/\omega^2)] . \tag{D.11}$$

The energy passed by a slit of width "2a" centered on the gaussian beam is given by

$$\text{Energy}_{slit} = (\pi\omega^2/2)\, E_0^2\, [2F(2a/\omega) - 1] , \tag{D.12}$$

where F(x) is the cumulative normal distribution mentioned in Appendix C. Note that $F(\infty)=1$ so that Eq. D.12 reduces to Eq. D.10 in the limit of an infinitely wide slit. Equations D.11 and D.12 are appropriate for calculating the energy coupled into a hollow cylindrical waveguide and a parallel-plate waveguide, respectively. Note that from Eq. D.11, the diameter of an aperture to transmit 99% of the energy is $\pi\omega$, but that a diameter greater than 4.6ω is required to reduce ripples in the far-field intensity pattern to less than 1% (Ref. 23). This strictly applies only to apertures and not to waveguides.

D.3 HOLLOW CYLINDRICAL WAVEGUIDE

The EH_{1m} modes are zeroth order Bessel functions, $J_0(u_{1m}r/a)$, where u_{1m} is the m'th zero of $J_0(x)$. The electric field of the gaussian beam can be written as

$$\exp(-r^2/\omega^2) = \sum_{m=1} c_m\, J_0(u_{1m}r/a) . \tag{D.13}$$

In writing this expression we assume that the beam waist (ω) of the gaussian beam is located at the entrance of the waveguide. The coupling coefficients, c_m, are found by multiplying both sides of Eq. D.13 by $J_0(u_{1m}r/a)\, r\, dr$ and then integrating over r from 0 to a to get

$$a^2 I_m(\omega/a) \equiv a^2 \int_0^1 \exp[-t^2(a/\omega)^2]\, J_0(u_{1m}t)\, t\, dt \tag{D.14}$$

$$= c_m\, (a^2/2)\, [J_1(u_{1m})]^2 ,$$

so that

$$c_m = 2\, I_m(\omega/a) \,/\, [J_1(u_{1m})]^2 \,. \qquad (D.15)$$

Now we can calculate the amount of energy coupled into each mode as a fraction (f_m) of the energy in the input gaussian beam. Substitute the c_m from Eq. D.15 into Eq. D.13, square both sides and integrate over the circular aperture of the waveguide to get

$$1 - \exp(-2a^2/\omega^2) = (8a^2/\omega^2) \sum_{m=1} [I_m(\omega/a)/J_1(u_{1m})]^2 \equiv \sum_{m=1} f_m \,. \qquad (D.16)$$

By an appropriate choice of the ratio ω/a we can couple most of the energy into the first mode (m=1). For ω/a set at 0.7063, f_1 is approximately 0.9704 and f_2 is zero, i.e. more than 97% of the gaussian beam energy couples into the first mode and no energy is coupled into the second mode. As the total energy coupled into the waveguide is 0.9819 ($= \sum_{m=1} f_m$) of the gaussian beam, only 1.15% of the input energy is coupled into all the higher order modes. If we neglect all the higher order modes then the peak fluence in the waveguide is just the peak fluence of the first mode given by $(c_1 E_0)^2 \approx (0.8982)\, E_0^2$.

D.4 PARALLEL-PLATE WAVEGUIDE

In the parallel-plate waveguide only one dimension is guided. If we define the x-axis as the direction perpendicular to the plates, then we can locate the plates at x=−a and x=+a running parallel to the y-axis. From Eq. D.8b, the y-dependence of a gaussian beam coupled into a parallel-plate waveguide is unchanged. Thus, the problem of finding the coupling coefficients reduces to finding them for the x-dependence of the electric field. Reference 22 lists the TE_m modes in the appropriate form. The odd-order TE_m modes are sine functions and the even-order modes are cosine functions. As the electric field of the input gaussian beam is a symmetric function, only the symmetric even-order modes are excited. Thus, the x-dependence of the electric field of the gaussian beam can be written as

$$\exp(-x^2/\omega_x^2) = \sum_{m=0} c_m \cos[(m+1)\pi x/(2a)] \,. \qquad (D.17)$$

The complete expression for the magnitude of the electric field in the parallel-plate waveguide is then

$$E_{xy} = \exp(-y^2/\omega_y^2) \sum_{m=0} c_m \cos[(m+1)\pi x/(2a)] \,. \qquad (D.18)$$

Note that as the x and y dimensions of the beam are treated independently, we now have a case of a cylindrical wavefront, i.e. one set of beam parameters for each of the x and y dimensions. The beam size ω_x is the beam waist in the x direction located at the entrance of the waveguide. In the rest of this discussion, we shall denote ω_x simply by ω. The beam size ω_y corresponds to the y direction, but it is not necessarily a beam waist. Cylindrical focusing optics are required to manipulate the x and y dimensions independently, especially for refocusing the y dimension of the beam inside the waveguide in a multipass geometry. The coupling coefficients c_m are found by multiplying both sides of Eq. D.17 by $\cos[(m+1)\pi x/(2a)]\cdot dx$ and then integrating over x from −a to +a to get

$$2a \int_0^1 \cos[(m+1)\pi t/2] \exp[-t^2(a/\omega)^2]\, dt = c_m a \qquad (D.19)$$

As before for the hollow cylindrical waveguide, we can now calculate the energy coupled into each mode as a fraction (f_m) of the energy in the input gaussian beam. Square both sides of Eq. D.17 and integrate over x from −a to +a to get

$$2F(2a/\omega) - 1 = (a/\omega)\,(2/\pi)^{1/2} \sum_{m=0} (c_m^2) \equiv \sum_{m=0} f_m \,. \qquad (D.20)$$

Again, by an appropriate choice of the ratio ω/a we can couple most of the energy into the lowest order mode (m=0). For ω/a set at 0.7734, f_0 is approximately 0.9839 and f_2 is zero, i.e. more than 98% of the input gaussian beam is coupled into the lowest mode and no energy is coupled into the next higher mode. The total energy coupled into the waveguide is 0.9903 of the input beam, so only 0.0064 of the input beam energy is coupled into higher modes. If we neglect all the higher order modes then the peak fluence at the entrance to the waveguide is just the peak fluence of the lowest mode given by $(c_0 E_0)^2 \approx (0.9537)\, E_0^2$.

Another choice of ω/a, 0.705, couples the greatest fraction of the gaussian beam energy, 0.9894, into the lowest mode and only 0.0060 into all the higher modes. Neglecting the coupling of energy into the higher order modes, the peak fluence of the lowest mode is $(0.8742)\ E_o^2$. The expression for the energy in the lowest mode is

$$E = (2/\pi)^{1/2}\ (a/\omega)\ c_o^2\ (\pi\omega\omega_y/2)\ E_o^2 \qquad \text{(D.21a)}$$

$$= a\ \omega_y\ (\pi/2)^{1/2}\ c_o^2\ E_o^2 \qquad \text{(D.21b)}$$

$$= a\ \omega_y\ (\pi/2)^{1/2}\ \Phi_{peak}\ . \qquad \text{(D.21c)}$$

Note that if ω/a is less than 0.44 then the parallel-plates are no longer effective as a waveguide, and the gaussian beam will propagate as if in free space. In this condition the parallel-plate waveguide has become an open cell as described in Appendix E.

D.5 HIGHER ORDER MODES

Although the total energy in the higher order modes is negligibly small, these modes have a significant effect on the intensity profile of the beam propagating in a waveguide. A computational study of a hollow cylindrical waveguide revealed intensity excursions of 50% or more from the profile of the lowest mode, even for the "single-mode" coupling quoted above. The computation followed the contributions of the first 20 modes and correctly incorporated the different propagation velocity and attenuation[22] for each mode based on the complex refractive index for glass.[24] For most cases only 10 modes were necessary for an accurate picture of the intensity profile. Experimental studies of beam propagation in waveguides are needed to determine the intensity distributions for a range of coupling conditions. This work could be carried out in parallel with studies of dissociation in waveguides as a further measure of the intensity distribution and to assess the efficiency of waveguides as photoreactors.

APPENDIX E

MULTIPASS CELL DESIGN: OPEN OR PARALLEL-PLATE WAVEGUIDE

An initial attempt to design a multipass cell is contained in the spreadsheet MPCELL.WR1. The intention was to examine cell designs that could be built and tested in our laboratory. The basic concept is that a gaussian laser beam enters the interaction volume of a cell and traverses the cell in several passes by reflecting off internal focusing mirrors at the end of each pass. The focal lengths of the mirrors are determined by the condition that the initial fluence (Φ_o) of the beam must be obtained at the end of every pass after allowing for mirror reflectivity and attenuation by the reactant gas in the cell. Thus, the beam must also be focused (mode-matched) into the cell initially. As Φ_o probably exceeds the damage threshold of the window materials, the entrance and exit windows of the cell are assumed to be located an appropriate distance away from the interaction volume. This spreadsheet does not include calculations for the entrance and exit portions of the cell; they are common to every photoreactor.

Two cell types are included: an open cell and a parallel-plate waveguide cell. The open cell encloses the minimum volume consistent with free-space propagation of the gaussian beam inside the cell. A good approximation to this condition is obtained by setting the transverse dimensions of the cell at no less than 4.6 times the beam radius at any point.[25] Thus, any aperture including the diameters of the spherical mirrors at the end of every pass must be at least 4.6ω.

The parallel-plate waveguide consists of two metal plates spaced a distance "2a" apart. The coupling of the gaussian beam into the waveguide depends on the ratio ω/a, and is assumed to be into the lowest order mode only. The non-guiding dimension of the waveguide must allow for free-space propagation, i.e. apertures at least 4.6 times the beam radius in that dimension. This applies especially to the cylindrical focusing mirrors at the end of every pass.

Section 1: A1..I20

```
  MULTIPASS CELL DESIGN FOR A GAUSSIAN BEAM
>  lambda      1076 1/cm     wavelength
>   press        60 torr     pressure          4.86E-06 mol/cm^3
>    temp       198 K        temperature       2.92E+18 molecules/cm^3
    alpha 3.35E-04 1/cm      <=attenuation=>   1.14E-22 cm^2/molecule
                                                  68.9 cm^2/mol
>      Lc       200 cm       cell length
> Phi.not        20 J/cm^2   minimum peak fluence (at ends)
>       n         5          No. passes
>      MR      0.99          mirror reflectivity
    Enot      2.70 J         minimum initial pulse energy

>    NTDL         1          N times diffraction limited
>   E.fac      1.02          energy factor for real beams
      Ein      2.76 J        initial pulse energy
>   Phi.L         1 J/cm^2   laser output fluence
       wL      1.31 cm       laser output beam radius
       En      1.90 J        final pulse energy
               31.3 %        energy utilization
>  switch         1          +1 or -1: pos. or neg. solutions
```

The ">" in the leftmost column indicates an input parameter. The first six lines of the spreadsheet specify the wavelength of the laser, and the conditions of the gas in the cell. The formula for the gas attenuation is taken from Eq. F.3. The next five parameters specify the cell length (L), the initial peak fluence of the laser beam (Φ_o), the number of passes in the cell (n), the mirror reflectivity (M), and an estimate of the minimum initial pulse energy required to obtain the minimum fluence at the end of every pass (E_o). Some insight into the beam propagation is provided by developing the formula for this estimate.

In the limit of no energy losses either by gas attenuation or mirror reflectivity, the condition of equal fluence at each mirror would require a constant beam size at the end of every pass. From symmetry and the necessity of focusing the beam, there would be a beam waist halfway along every pass. From Eqs. D.2 and

D.4, the beam waist that gives the minimum beam size at a distance L/2 corresponds to a Rayleigh range of just L/2. This is analogous to a symmetric confocal resonator. Thus, the Rayleigh range for the n'th pass (indeed for every pass in this case) would be exactly half the length of the cell, and the beam size at the end of the n'th pass (ω_n) would be given by

$$\omega_n^2 = L\lambda/\pi \; . \qquad \text{(E.1)}$$

The beam energy at the end of the n'th pass is

$$E_n = (\pi\omega_n^2/2)\,\Phi_0 \qquad \text{(E.2)}$$

from the definition of the peak fluence Φ_0. Allowing for beam attenuation again we obtain

$$E_n = M^{n-1}\,E_0\,\exp(-n\alpha L) \qquad \text{(E.3)}$$

from the initial pulse energy E_0 attenuated by n−1 mirror reflections and by n passes of length L through the gas in the cell. From Eqs. E.1 to E.3, we obtain an estimate of the minimum initial pulse energy;

$$E_0 = (L\lambda/2)\,\Phi_0\,\exp(-n\alpha L)/M^{n-1} \; . \qquad \text{(E.4)}$$

Of course, more energy will probably be necessary, so the next group of parameters includes an "energy factor for real beams", "E.fac". This is a multiplier for E_0 to obtain "Ein", the initial pulse energy. The parameter "NTDL" (N) allows for non-diffraction limited beams. To estimate the size of laser needed to produce Ein, the laser output beam radius is calculated from the laser output fluence. The final pulse energy is E_n given by Eq. E.3 with Ein replacing E_0. The energy utilization is just the fraction of energy lost to the cell. The final parameter in the list is "switch", which is used in the solution of the beam parameters for the multipass cells illustrated in the next two sections.

Sections 2 and 3 are located side by side in the spreadsheet. Section 2 displays the beam sizes and beam parameters obtained by solving Nemoto's equations.[21] Section 3 contains the parameters defined by Nemoto to solve for the beam waist and Rayleigh range of a beam given the beam sizes at two points. In this case the two points are the start and end of a pass. The examples below illustrate the solution for 5 passes in both the open cell and the parallel-plate waveguide.

Section 2: A22..L39

A	B	C	D	E	F	G	H	I	J	K	L
#	E.init	w.start	w.end	w.0	Rayleigh	z0	NTDL	focus	f0	d1	b1*b2
	J	cm	cm	cm	cm		limit	cm	cm	cm	cm^2
1	2.76	0.296	0.285	0.269	244.1	113.4	1.20	318.2	230.8	86.6	53278
2	2.55	0.285	0.274	0.254	218.2	111.1	1.15	261.4	205.1	88.9	42056
3	2.36	0.274	0.264	0.239	192.7	109.1	1.11	211.1	179.1	90.9	32078
4	2.19	0.264	0.254	0.222	166.5	107.3	1.06	166.2	152.1	92.7	23121
5	2.03	0.254	0.246	0.203	138.9	104.9	1.03				
	1.90	0.246									
parallel-plate			(w/a)	c.0	a						
			0.705	0.935	0.393						
1	2.73	0.277	0.267	0.243	199.2	109.6	1.12	223.4	185.8	90.4	34524
2	2.53	0.267	0.257	0.226	173.3	107.7	1.08	176.1	158.5	92.3	25126
3	2.34	0.257	0.247	0.207	145.0	106.0	1.03	ERR	ERR	94.0	ERR
4	2.17	0.247	0.238	ERR	ERR	ERR	1.00	ERR	ERR	ERR	ERR
5	2.01	0.238	0.230	ERR	ERR	ERR	0.96				
	1.88	0.230									

Found in column A in Section 2 is the number of the pass. Columns B and C give the beam energy at the start of the pass calculated according to Eq. G3, and the corresponding beam size calculated from Eq. G2. The beam size at the end of a pass is identical to that at the start of the next pass, and is listed in column D. From the two beam sizes, we obtain the beam waist ("w.0") and waist location ("z0") listed in columns

E and G. The Rayleigh range in column F is calculated from the beam waist and allows for NTDL beams (see Appendix D). The NTDL limit listed in column H indicates that a non-diffraction limited beam could be accommodated with the same beam sizes at the ends of the pass. It is calculated from $N/r^{1/4}$, where r is one of Nemoto's parameters. Note that the only NTDL limit that matters is the one for the final pass. The final four columns in Section 2 concern the matching of the beam to the next pass. The parameter "b1*b2" defined by

$$\text{"b1*b2"} = [\pi\, \omega_{0i}\, \omega_{0,i+1} / (N^2\, \lambda)]^2 , \tag{E.5}$$

where ω_{0i} and $\omega_{0,i+1}$ are the beam waists for the i'th and (i+1)'th pass, is used to calculate the focal length of the common mirror. The square root of "b1*b2" gives "f0", the minimum focal length that can match the two beam waists. The distance from ω_{0i} to the mirror is "d1", given by $L-z_0$. If we take "d2" as the distance from the mirror to $\omega_{0,i+1}$, which is just z_0 for the (i+1)'th pass, then the required focal length is

$$\text{"focus"} = f \equiv (b1*b2 + d1 \cdot d2) / (d1 + d2) , \tag{E.6}$$

found in column I.

In the example solution for the parallel-plate waveguide, all the formulas are the same as for the open cell except for the initial energy and the beam size at the start of each pass. Two extra input parameters are needed also: ω/a and c_0 (see Appendix D). The half-separation of the plates, a, is calculated from ω/a and the initial beam size. The initial energy is given by Eq. D.21a;

$$E = (2/\pi)^{1/2}\, (a/\omega)\, c_0^2\, E_m , \tag{E.7}$$

where E_m is the gaussian beam energy. The beam size calculation corresponds to the y-dimension only. From Appendix D, the beam size in the parameter ω/a is the beam size in the x-dimension. If we label the beam sizes by their corresponding dimensions then the initial peak fluence is given by (see Eq. D.21c)

$$\Phi_0 = (2/\pi)^{1/2}\, E / (a\omega_y) \tag{E.8}$$

$$= (2/\pi)^{1/2}\, [E / (\omega_x \omega_y)]\, (\omega_y/a) .$$

Any assumption on the relation between ω_x and ω_y provides a solution for the beam size from this equation. We have assumed that the initial beam size is the same in both dimensions.

The entries marked "ERR" in the example for the parallel-plate waveguide indicate that there is no solution for that entry. A larger input energy, obtained by increasing "E.fac" or by decreasing N, will remedy this situation. The key to the existence of a solution is that the parameter "r" be less than or equal to 1.

The last four columns of Section 3 list the parameters defined by Nemoto to solve for the beam waist and location. The parameters z1, z2, u and v grouped at the top of these columns are common to all the solutions as they depend only on the length of the cell. The first three columns provide a numerical check on the solutions by calculating d1 and the beam sizes at the ends of the passes from independent formulas. The formula for d1 is taken from Eq. 9 of Ref. 15 and modified to account for NTDL beams:

$$d1 = f - [\pm\pi\, (\omega_0/N)^2 / \lambda]\, [f^2 / (b1*b2) - 1]^{1/2} . \tag{E.9}$$

The formula to check the beam sizes is just the beam divergence formula, Eq. D.2.

Section 3: M21..S38

**** CHECKS ****			z1	0	u	200
d1	w.start	w.end	z2	200	v	-200
(from f)	(from z0 and w0)		p	q	r	t
86.6	0.296	0.285	2.00	0.08	0.49	-207.85
88.9	0.285	0.274	2.00	0.08	0.57	-207.85
90.9	0.274	0.264	2.00	0.08	0.67	-207.85
92.7	0.264	0.254	2.00	0.08	0.78	-207.85
	0.254	0.246	2.00	0.07	0.90	-206.81
90.4	0.277	0.267	2.00	0.08	0.64	-207.85
92.3	0.267	0.257	2.00	0.08	0.75	-207.85
ERR	0.257	0.247	2.00	0.08	0.87	-207.85
ERR	ERR	ERR	2.00	0.08	1.02	-207.85
	ERR	ERR	2.00	0.07	1.18	-206.81

APPENDIX F

EQUIFLUENCE CELL MODEL FOR COST ESTIMATION

The spreadsheet EQCELL.WR1 was used to estimate the laser costs for large scale application of laser tritium separation, i.e. the 500 kg/h plant for tritium production at NET. Some of the parameters used here have since been modified or replaced. A sample of the spreadsheet calculation is provided here to aid in the explanation of its operation.

Section 1: A1..H6

```
  LASER TRITIUM SEPARATION IN EQUIFLUENCE CELLS
I:        F    38375.0 moles/h  CF3H feed
I:   Fwater      500.0 liter/h  water feed
I:     Tppm        4.30 ppm     Input T in CF3H
I: (T/CF3H)        0.43 ppm     Output T in CF3H (after make-up)
      Gdep        0.10 gas depletion required
```

The "I:" in the first column indicates that the adjacent parameter is an input variable and not a formula. Thus, "F" is the input variable for the CF_3H feed stream in moles/h, "Fwater" is the water stream input, "Tppm" is the tritium concentration (f in Eq. 1) in the CF_3H stream from the exchange towers, and "(T/CF3H)" is the tritium concentration in the CF_3H after the photoreactor and after adding CF_3H to make up for all the gas that has been dissociated. The parameter "Gdep" is 1-Q (see Eq. 1) given by the ratio of the output to input tritium concentrations.

Section 2: A7..I17

```
                                                 LASER POWER
I:       dT        0.50 dissociation rate of T     334.562 kW        906.418 kW
I:        S       10000 Selectivity                  0.444 mmol/kWh
         dH    5.00E-05 dissociation rate of H              Complete mixing
         np       3.322 laser pulses per gas fill               npm     9.000
   (NRT/NT)    1.00E-01 T remaining                      (NRT/NT) 1.00E-01
   (NRH/NH)    0.999834 H remaining                      (NRH/NH) 0.999550
                              <--No Mixing
   (NTF/NT)    0.900000 T as TF          Mixing -->      (NTF/NT) 0.900000
   (NHF/NH)    0.000166 H as HF                          (NHF/NH) 0.000450
             5418.85 Enrichment                                      2001

    Make-up       6.52 mol/h    HF+TF production = CF3H make-up        17.41
      (T/QF)      2.28 %        Output T concentration in QF            0.85
                  0.15 mol/h    Production of T                         0.15
```

The input parameters here are "dT", the average probability of CF_3T dissociation per pulse denoted by ε_v in Eq. 6, and "S", the dissociation selectivity of CF_3T over CF_3H. Thus, "dH = S/dT" is the probability of dissociation of CF_3H. The two limiting cases of gas flow are treated: "No mixing" or plug flow (column C), and "Mixing" or stirred flow (column I), with "np" and "npm" as the corresponding average gas residence times denoted by t in Appendix B. The various parameters listed below "np" and "npm" are the fractions of T as CF_3T, H as CF_3H, T as TF, and H as HF in the product stream. Note that the latter two are just the required tritium depletion Q and the corresponding depletion for H. The ratio of these two depletions yields the "Enrichment" factor of the product stream, also denoted by β. In the spreadsheet the formulas used for "(NTF/NT)" and "(NTH/NH)" in the case of complete mixing derive from the expression for Q in Appendix B. The calculation of these two parameters employs two additional spreadsheet cells, J15 and J16, not shown above. The amount of CF_3H needed for "Make-up" is identical to the amount of TF and HF created, and calculated by the formula

$$M = F\,[\,Qf + Q(1-f)/\beta\,]\,. \qquad \text{(F.1)}$$

The rate of tritium production is just the first term of Eq. F.1, or FQf. The tritium concentration in the product stream, ρ, is the ratio of the two, so

$$\rho = \beta f / [\, \beta f + (1-f) \,] . \qquad \text{(F.2)}$$

The formulas in the spreadsheet cells appear more complicated than this because of the way they were developed originally, but they are equivalent to the formulas above.

Also appearing in Section 2 as aids for analysis are the total laser power required in kilowatts and the production rate of tritium in millimoles per kilowatt-hour. The laser power is calculated later in the spreadsheet.

Section 3: A22..H24

```
I         T        198 K         temperature of CF3H
I     ptorr         60 torr      input pressure of CF3H
      Vflow  2.19E+03 liter/s     CF3H volume flow (7901.920 m^3/h)
```

The pressure and temperature of the gas in the photoreactor determine the total volumetric flow rate, V_{sccm}, of the feed stream F. The next section calculates the geometry and dimensions of the equifluence cells that make up the photoreactor. The total gas flow is divided among several cells operating in parallel, and in each cell the gas flows transversely to the laser beam.

Section 4: A26..I45

```
I        Nw         20           number of cells
I       rep      300.0 Hz       laser repetition rate
I      frac        0.9           fraction of laser energy used
I     npass          5           number of passes of beam in cell
I        mr       0.99           mirror reflectivity in cell
C     atten     0.0335 1/m       laser energy atten. coeff.
         red     0.6310           single-pass energy reduction
      funcfn     1.9438           processing area factor     26.15324
      area.b       0.46 cm^2      initial area of beam                    1.26
           L      13.45 m         length of cell
       Vcell  1.22E+03 cm^3       cell volume                      3.29E+03
      area.c       0.90 cm^2      area of cell                            2.45
         Dmm       10.7 mm        diameter of cell                       17.7
                   3.32           cell to flow ratio := np (or npm ->)      9
                  67.27 m         total path length
I      phiC         40 J/cm^2      critical fluence for dissociation
      Power     334562 W          total laser power (equiv. long pulse  906418
    Power.m      16728 W          laser power per cell                   45321
     Energy       18.6 J          laser pulse energy per cell             50.4
                     3            factor for equivalent long pulse
```

Section 4 calculates the dimensions of an ideal equifluence cell as part of the photoreactor: the first five rows and row 41 provide input. The photoreactor is considered as "Nw" (or N_w) single equifluence cells in parallel, each with it's own laser operating at "rep" (or R) Hz. Each cell consumes a fraction "frac" (or f) of the input laser power by multi-passing the laser beam "npass" (or n) times using internal mirrors with a reflectivity "mr" (or π_r). The laser beam is also attenuated by absorption in the gas according to Beer's Law, where "atten" is the 1/e absorption length. The expression for "atten", also denoted by α, was obtained from absorption measurements in CF_3H as a function of pressure under conditions of low laser power and a gas temperature of 197 K (see Fig. 2):

$$\alpha = [\, 9.016(p/T) + 6.707(p/T)^2 \,] \times 10^{-2}\ m^{-1}. \qquad \text{(F.3)}$$

The temperature dependence in this formula is only valid near 197 K. This expression also may not be valid for high fluence pulses, as revealed by measurements in April 1989 (Fig. 2). The reduction in laser

energy per pass is the factor "red" or r, which is defined by $(1-f)^{1/n}$. Then the length of the cell is given by

$$L = -(1/\alpha)\ \ln(r/m)\ . \qquad \text{(F.4)}$$

In the simple dissociation threshold (SDT) model any CF_3T exposed to fluences greater than or equal to the critical fluence for dissociation, "phic" (read ϕ_c), is dissociated by a single pulse. Thus, the area of the cell is calculated on the assumption that the laser beam fluence is constant everywhere along its path. The reduction in laser energy by attenuation and mirror reflection is compensated by reducing the area of the beam. Note that this treatment completely ignores diffraction and the usual beam propagation formulas. The initial area of the beam is "area.b" (or b) defined as the ratio of the laser pulse energy to ϕ_c. The parameter "funcfn" (or f) represents the number of bL volumes required to process the gas in one cell. It is derived by integrating the volume of a single pass and summing the volumes over the number of passes. If the initial beam area of the i'th pass is a_i $(= b{\cdot}r^{i-1})$ then the final area is $a_i{\cdot}r$ or $a_i{\cdot}m{\cdot}\exp(-\alpha L)$. Therefore, the beam area at any position z along the pass is $a_i{\cdot}m{\cdot}\exp(-\alpha z)$. Integrating this expression from 0 to L gives the volume V_i as $a_i{\cdot}m{\cdot}[1 - \exp(-\alpha L)]/\alpha$, or $a_i(m-r)/\alpha$ by the definition of r. The volumes V_i make a series of constant ratio r with initial value $b(m-r)/\alpha$. The sum of the series is "Vcell" (or V_c) given by

$$V_c = b\ [(m - r)/\alpha]\ [(1 - r^n) / (1 - r)]\ , \qquad \text{(F.5a)}$$

$$= b\ \{(m - r)/(\alpha L)\ [f / (1 - r)]\}\ L\ , \qquad \text{(F.5b)}$$

using the definition of f and including the cell length. The expression in braces is f and the product of f and b is "area.c" on the condition that f is not less than 1. If f is less than 1 then V_c is just bL. The diameter of a cylindrical cell of volume V_c and length L is given in millimeters by "Dmm". The row below "Dmm" provides a check on the calculation of the cell volume by calculating the average residence time of the gas in V_c from

$$t = V_c\ R\ N_a / V_{sw}\ , \qquad \text{(F.6)}$$

i.e. it should be "np" and "npm" for the two cases. The value in the next row is simply the total path length of the laser beam in the equifluence cell.

In Section 4 the number 26.15324 appearing in spreadsheet cell H33 is the product of f and L; recall from Eq. F.5b that V_c is bfL. The total laser power, P_T, is obtained from this expression for V_c by replacing b with E/ϕ_c where E is the laser energy per pulse given by $P_T/(R{\cdot}N_a)$, and by substituting $V_{sw}{\cdot}t/(R{\cdot}N_a)$ for V_c:

$$P_T = V_{sw}\ t\ \phi_c\ /\ (fL)\ . \qquad \text{(F.7)}$$

Row 45 of the spreadsheet provides an efficiency factor, i.e. 3 in the sample above, for the laser energy in the normal long pulse of the TEA CO_2 laser relative to a shorter pulse. The example is for the 50-100 ns pulse obtained by reducing the nitrogen content of the laser gas mixture to eliminate the long tail. This factor multiplies the expression for power in Eq. F.7 to obtain the total optical power required of the equivalent long pulse laser system, but is removed again in calculating the laser pulse energy per cell.

Section 5: A46..I54

```
   9.91 M$        Laser capital cost, first year

0.7037 $/Ci       T cost
  6.09 $/liter    total processing cost
  8.66 Ci/liter   T production

  5.35 $/liter    electricity cost of processing feed
  0.74 $/liter    system cost of processing feed (capitalised)
0.0037 $/liter    CF3H makeup (cost per liter of feed) @$4/kg
```

The first line of Section 5 estimates the capital cost in the first year of the laser system for this photoreactor design: this is just the "total laser system capital cost" multiplied by the "accessories factor", both described

in the next section. The "T cost" is the ratio of the "total production cost" to the amount of "T production" expressed in Ci/liter (of feed water). The total processing cost is the sum of the operating costs for electricity and CF_3H make-up and the capitalized cost (at 10% over 15 years) of the laser system, neglecting the costs of the photoreactor.

Section 6: A57..H66

SYSTEM	24912	$K	system lifetime cost
facc	1		accessories factor
QCDC	20		number of lasers
LHCDC	3304	$K	laser capital cost
PSCDC	6608	$K	power supply cap. cost
CAPCOST	9911	$K	total laser system capital cost
eff	0.1		electrical efficiency
eprice	0.04	$/kWh	electricity price
	29.63	$/W	average capital cost of laser power

The "SYSTEM" cost is the sum of the total laser system capital cost, "CAPCOST", and the total laser system replacement cost, "REPCOST" (shown below), multiplied by the accessories factor, which has been set to 1 here. The capital and replacement costs are estimated by expressions found in Ref. 25. The laser system capital cost is the sum of the laser head, "LHCDC", and power supply costs, "PSHDC":

$$LCHDC = 1.792\ (POWER)^{0.512}\ (QCDC)^{0.848}\ , \text{ and} \qquad (F.8)$$

$$PSHDC = 3.584\ (POWER)^{0.512}\ (QCDC)^{0.848} \qquad (F.9)$$

where POWER is the optical power (for long pulses) of each laser and QCDC is the number of lasers, identical to N_L above. An electrical efficiency of 10% is assumed for the (long pulse) lasers, and a unit price of 0.04$/kWh, too low now. The average capital cost of laser power is calculated to compare it with estimates of laser costs obtained from other sources.

Section 7: A68..H80

QLCDR	47.3		laser heads
LHCDR	5941	$K	laser replacement
MTBFH	50000	hours	between failures
LLIS	15	years	system lifetime
FOP	0.9		fraction time operating
RFCDH	1		laser replacement factor
QPCDR	35.4		power supplies
PSCDR	9059	$K	supply replacement
MTBFP	6690	hours	between failures
RFCDP	0.1		supply replacement factor
REPCOST	15000	$K	total laser system replacement cost

The expressions for the terms to calculate the total laser system replacement cost are as follows:

$$QLCDR = (LLIS \times 24 \times 365 \times FOP / MTBFH) \times QCDC \times RFCDH\ , \qquad (F.10)$$

$$LHCDk = LHCDC \times \{[(QCDC + QLCDR) / QCDC]^{0.848} - 1\}\ , \qquad (F.11)$$

$$QPCDR = (LLIS \times 24 \times 365 \times FOP / MTBFH) \times QCDC \times RFCDP\ , \qquad (F.12)$$

$$PSCDR = PSCDC \times \{[(QCDC + QPCDR) / QCDC]^{0.848} - 1\}\ , \qquad (F.13)$$

$$REPCOST = PSCDR + LHCDR\ . \qquad (F.14)$$

In Eq. F.10 and F.12, "MTBFH" is the mean time between failures, "LLIS" is the lifetime for the system, and "FOP" is the fraction of time the system will be operating properly. The replacement factors, "RFCDH"

and "RFCDP", refer to the fraction of the laser head and power supply, respectively, that will need to be replaced after a failure.

The spreadsheet contains some additional expressions for estimating other costs of the laser system also obtained from Ref. 25, but they were never used.

Section 8: K9..M15

```
          SEPARATOR
          at 5 atm  temp(C)
QF/CF3H                    0
  input   6.5E-01 torr
 output   1.4E-04 torr
TF/CF3H
 return   8.1E-04 ppm
```

For completeness, the spreadsheet includes a calculation for the operation of the TF separator. The temperature is an input variable referring to the temperature of the sodium fluoride beds. The input partial pressure is calculated from the quantity of TF and HF produced and assuming a pressure of 5 atm in the separator. The output partial pressure of TF and HF is calculated from

$$\log_{10} p = 6.946 - 3739/T \qquad \text{(F.15)}$$

where p is the pressure in atmospheres and T is the absolute temperature in Kelvin. Finally, the output partial pressure is converted into parts per million.

Section 9: K27..R34

```
coll. frequency Z 1.10E+09

        R   8.3145 J/mol/K  Gas constant
        M 0.070014 kg/mol   CF3H molar mass
       mu 9.25E-06 Pa.s     absolute viscosity of CF3H
     rhol    0.340 kg/m3    density of CF3H
      vel     0.76 m/s      CF3H velocity: transverse flow per cell
       Re      300          Reynold's number
```

Some constants of CF_3H are listed in Section 9 along with expressions for the viscosity μ to calculate the collision frequency Z and Reynold's number Re for transverse flow in the equifluence cells. The viscosity expression was obtained from data sheets on Freons by Dupont:

$$\mu = (1.747\ T^{0.5} - 15.33) \times 10^{-6} \quad \text{Pa·s} . \qquad \text{(F.16)}$$

I do not recall the source for the collision frequency expression, but it can be checked in most texts on kinetic theory of gases:

$$Z = 169.4\ (p/\mu) \quad s^{-1} , \qquad \text{(F.17)}$$

where p is the pressure in torr. The transverse flow velocity is the gas flow for one cell divided by the transverse area, which is the length times the cell diameter. The Reynold's number is calculated using the cell diameter as the typical length parameter.

Section 10: A116..H127

```
  COMPRESSION COSTS
I:    gamma        1.4 ratio of specific heats
I:     p.hi          5 atm
       p.lo         60 torr
     pratio      63.33
     Tratio       3.27
       Tgas        198 K
      T2gas        648 K
       Work      13088 J/mol
         TR         70 %          compressor efficiency
    WorkCE      199.3 kW
                0.0159 $/liter   compression cost
```

This final section in the spreadsheet is an attempt to estimate the cost of gas compression based on formulas found in Perry's Handbook for Chemical Engineers. In the process flowsheet the gas must be compressed after the photoreactor and before the separator. Note that the high pressure is an input parameter set here to 5 atm. The parameters "p.lo" and "Tgas" are just the pressure and temperature of the gas in the photoreactor defined much earlier in the spreadsheet. The "pratio" is the ratio of the high to low pressures, and "Tratio" is defined by "pratio" raised to the power of $(1-1/\gamma)$ where γ is the ratio of specific heats. The parameter "T2gas" is the temperature of the compressed gas defined as the product of "Tratio" and "Tgas". The work done is given by

$$\text{Work} = R\,T\,(T_{_} - 1)\,\gamma\,/\,(\gamma - 1) \quad \text{J/mol} \qquad \text{(F.18)}$$

where R is the gas constant. From the compressor efficiency and the gas feed rate we can calculate the total electrical power required for gas compression, listed as "WorkCE". Finally, the electrical operating cost per liter of water feed is obtained from "WorkCE" and the unit price of electricity.

APPENDIX G

CYLINDRICAL WAVEGUIDE CELL MODEL FOR COST ESTIMATION

The spreadsheet SEPCOST.WR1 models a cylindrical waveguide cell as a unit of the photoreactor for laser-based tritium separation. A copy of this spreadsheet was later modified and renamed as EQCELL.WR1 to model the equifluence cell for the photoreactor. Thus, most of the parameters and expressions in SEPCOST.WR1 have been explained already in Appendix F. The description below concentrates on the differences in the two spreadsheets as they affect the treatment of a cylindrical waveguide cell.

In SEPCOST.WR1 there are no helpful reminders to distinguish input variables from calculated parameters. Many of the input variables are the same as in EQCELL.WR1, but the first difference is found in "dT", the dissociation rate of CF,T. A table of dissociation rates was computed for a waveguide cell based on the model of Dr. O'Neill. In the cylindrical waveguide cell the laser beam is assumed to propagate in the fundamental mode EH_{11}, which is a Bessel function of order zero with its first zero at the wall of the cylinder. On input the peak intensity of the laser beam is set equal to the breakdown fluence of the gas. The waveguide walls and the gas in the cell attenuate the laser beam as it propagates. The simple dissociation threshold (SDT) model is applied to determine the fractional volume of the cell in which dissociation occurs. Obviously, the critical fluence for dissociation must be less than the breakdown fluence of the gas for any dissociation to occur. Section R1..U130 lists the dissociation probabilities computed for breakdown fluences in the range of 80 to 150 J/cm² with the critical fluence for dissociation in the range of 40 J/cm² up to the breakdown fluence. (I have not checked the validity of these numbers for this report, but they are approximately correct and certainly good enough for demonstrating the operation of this spreadsheet.) This list was copied into a table in section X4..AE25 to exploit the @INDEX function of Symphony. Thus, the value for "dT" depends on the selection of breakdown fluence and of the critical fluence for dissociation in the spreadsheet cells G10 and G11, respectively. As the gas flows down the cylindrical waveguide it is irradiated by a number of pulses, "np". The input for "np" is either B5 or H39 depending on whether the value of cell C5 is 1 or not. The depletion of CF,T is calculated by the formula for plug flow.

Section 1: A1..H20

```
      dT   1.46E-01 dissociation rate of T              SEPARATOR
       S      10000 Selectivity                         at 5 atm, -60C
      dH   1.46E-05 dissociation rate of H      QF/CF3H                    0
      np       15.1 number of laser pulses        input  8.5E-01 torr
               15.1          1                   output  1.4E-04 torr
(NRT/NT)   9.28E-02 fraction of T remaining     TF/CF3H
(NRH/NH) 0.99978002 fraction of H remaining      return  6.1E-04 ppm

   Tppmw        3.0 ppm      T in water        DISSOCIATION CELL FLUENCES
    Wdep   1.00E-01 water depletion             Breakdown     100 J/cm2
   (G/L)        0.7 CF3H/liquid flow            Threshold      40 J/cm2
    Tppm       4.26 ppm      T in CF3H           Iratio    0.392 (2% loss)
    Gdep   9.37E-02 gas depletion required                 0.782 kW.h/l
     tbr     1.3298 tower bottom ratio: (NRT/NT)/Gdep = 0.989561
                                                          8.75 Ci/l
  Fwater        500 liter/h  water feed
       F      38850 moles/h  CF3H feed
 Make-up       8.70 mole/h   HF+TF production = CF3H make-up
(T/CF3H)   3.95E-01 ppm      Output T concentration in CF3H (after make-up
  (T/QF)   1.73E+04 ppm      Output T concentration in QF
```

A satisfactory solution requires "(NRT/NT)" less than or equal to "Gdep"; the ratio of these two parameters is located in cell G14.

Section 2: J4..N5

```
(NTF/NT) 0.907244 fraction of T as TF
(NHF/NH) 0.000219 fraction of H as HF
```

Note that in this version of the costing analysis the concentration of CF_3T and the quantity of CF_3H feed is calculated from some basic input parameters for the exchange towers. It is better to handle the exchange towers separately and to provide the necessary inputs for analyzing the performance of the photoreactor as has been done in EQCELL.WR1.

Section 3: A23..F30

R	8.3145	J/mol/K	Gas constant
M	0.070014	kg/mol	CF3H molar mass
T	198	K	temperature of CF3H
mu	9.25E-06	Pa.s	absolute viscosity of CF3H
gamma	1.4		ratio of specific heats
vs	181.4	m/s	velocity of sound
Vflow	666.64	liter/s	CF3H volume flow
rhol	1.134	kg/m3	density of CF3H

The velocity of sound in CF_3H provides an upper limit for the gas flow through the cylindrical waveguides. Note that the total volume flow in this example is different from Appendix F because the gas pressure and temperature are different.

Section 4: A32..H43

ptorr	200	torr	input pressure of CF3H		
Nw	60		waveguides: 4 in parallel, reducing diameter		
Dmm	20	mm	diameter of largest waveguide		
L	5.74	m	length of waveguide(s)		
vel	26.99	m/s	CF3H velocity: for largest waveguide		
Re	66169		Reynold's number		
vmax	28.60	m/s	vl for deltap/ptorr=0.1	INPUT	
L/(D*Np)	19.0		>10 for proper mixing	Np	32
				Fwater	500
rep	71.0	Hz	laser repetition rate		
Energy	91.8	J	laser pulse energy (5% input loss)		
Power	6516	W	laser power		

Attenuation of the laser beam as it propagates down the cylindrical waveguide reduces the peak fluence. The maximum useful length of the waveguide is at the point where the peak fluence is equal to the critical fluence for dissociation: this defines "L" in the section above. The attenuation coefficient is provided in the next section. Although the fluence of the laser beam may be too low for dissociation in this first waveguide, the energy in the beam is not exhausted. To use the remaining laser energy the beam can be focused into a second smaller waveguide at an initial fluence again equal to the breakdown fluence of the gas. The spreadsheet allows up to four such waveguides to utilize the energy of one laser beam in series while the gas flows through in parallel. In this way the laser energy is used most efficiently and the gas flow processed by one laser is increased. Thus, "Nw" is the number of 4-waveguide sets, "Dmm" is the diameter of the largest waveguide in each set, and "L" is the length of each waveguide. The average gas velocity through the largest waveguide in each set is "vel", obtained by dividing the total gas flow by the number of sets and the effective cross-sectional area of each set. The factor for the effective area of the set relative to the largest waveguide is given below. The maximum gas velocity, "vmax", for the largest waveguide is defined as the velocity that requires a pressure drop of 10% over the length of the waveguide:

$$v_{max} = [(RT/M)\ (0.05)\ D\ /\ (L \cdot f_f)]^{1/2} \quad \text{m/s} \qquad \text{(G.1)}$$

where f_f is the friction factor for the waveguide material. This expression derives from Darcy's formula for the pressure drop in a pipe (see below). It was obtained from a handbook on flow in pipes published by Crane Engineering, and available in the Research Division library. Note that "vel" must be less than or equal to vmax; increase or decrease "Nw" until this relation is satisfied.

The repetition rate of the laser is required to be the reciprocal of the average residence time of gas in the largest waveguide, or "np" times "vel" divided by "L". The laser pulse energy is defined by the area of the largest waveguide and by the breakdown fluence. The exact formula for the pulse energy depends on

the coupling of the input beam into the waveguide and the window loss, taken here as 5%. The optical power of each laser is then just the product of the pulse energy and the repetition rate.

Section 5: A53..H57

```
      D   2.00E-02 m
  atten     0.0798 1/m      field atten. coeff.
     ff     0.0050          friction factor
 deltap       17.8 torr     p drop in pipe (Darcy's formula)
              22.5 torr     total pressure drop
```

For most formulas the diameter of the largest waveguide is more useful expressed in meters, D, than in millimeters, "Dmm". The field attenuation coefficient is the Beer's Law coefficient of attenuation for the electric field of the laser beam, and is the sum of two terms. The first term is the attenuation from the waveguide walls,[22] which for glass at a wavelength of 9.3 μm is $(1.859 \times 10^{-12} / D^3)$ m^{-1}. The second term accounts for absorption in the gas, updated here to use the expression from Eq. F.3 for intensity attenuation. Note that the attenuation coefficient for electric field is just half that for intensity. The friction factor refers to the resistance of the glass pipe to gas flow, and it depends on the Reynolds number of the flow:

$$f_f = 64 / Re \qquad \text{for } Re \le 2000, \tag{G.2}$$

$$\log f_f = -1.2691 - 0.214 \log Re \qquad \text{for } Re > 2000. \tag{G.3}$$

Darcy's formula (see $v_{__}$ above) provides "deltap", the first of two terms in the total pressure drop in the largest waveguide. The second term obtains from the kinetic energy of the gas. Darcy's formula is also applied to finding the gas velocity in the second, third and fourth waveguides. The diameters of these waveguides are obtained from the diameter of the first waveguide and successively applying the square root of the ratio of the critical fluence to the breakdown fluence. This ratio is provided in the spreadsheet as "Iratio" in Section 1 above.

Section 6: J31..P48

```
          WAVEGUIDES in PARALLEL
First      Second     Third     Fourth

      20     12.52      7.84      4.91 mm          diameter
    0.02     0.013     0.008     0.005 m          diameter
   26.99     21.36     16.90     13.37 m/s        velocity
   66169     32781     16240      8045 Reynold's number

       1    0.3102    0.0000    0.0000 rel. volume flow (V*D*D)
    15.1      19.1      24.1      30.5            average pulses
  0.0928    0.0495    0.0224    0.0082            depletion
9.28E-02  1.54E-02  0.00E+00  0.00E+00            flow*depletion
                                        0.1081 sum of flow*dep
                                        1.3102 sum of flows
Do not use if v*d*d<.1
                                      0.082523 average depletion
                                      0.152284 average dT
  0.0050    0.0058    0.0068    0.0079          friction factor
```

The gas flowing through the smaller waveguides encounters more laser pulses because of the slower gas velocity in these pipes. The average depletion of the gas flowing through one set of waveguides, obtained as the ratio of the sum of flow times depletion to the sum of flows, is used to calculate the average dissociation probability, dT, based on "np" pulses. This dT can then be compared to the input value of "dT" to evaluate the effectiveness of this configuration of waveguides. If the relative volume flow of a waveguide falls below 10% of the largest waveguide then it is excluded from the configuration. This implies that the diameters of the smaller waveguides must be greater than 40% of that of the largest waveguide. Although the friction factors for each waveguide are calculated, they are not yet included in the calculation of the gas velocity.

Section 7: A44..H51

```
0.1948 $/Ci      T cost
  1.70 $/liter   total processing cost
  8.75 Ci/liter  T production

  0.31 $/liter   electricity cost of processing feed
  1.39 $/liter   system cost of processing feed (capitalised)
0.0049 $/liter   CF3H makeup (cost per liter of feed) @$4/kg
 18.63 M$        Laser capital cost, first year
```

The costing formulas in SEPCOST.WR1 are identical to those in EQCELL.WR1.